Fall 2012

Configuration Studies of Electrostatic and Magnetostatic Active Space Radiation Shielding

Trac K. Nguyen
Old Dominion University

CONFIGURATION STUDIES OF ELECTROSTATIC AND MAGNETOSTATIC ACTIVE SPACE RADIATION SHIELDING

by:

Trac K. Nguyen
B.S. August 2008, Old Dominion University

A Thesis Submitted to the Faculty of
Old Dominion University Partial Fulfillment of the
Requirements for the Degree of

MASTER OF SCIENCE

ELECTRICAL ENGINEERING

OLD DOMINION UNIVERSITY
December 2012

Approved by: //

R. P. Joshi (Director)

L. L. Vahala (Member)

M. Thitsa (Member)

ABSTRACT

CONFIGURATION STUDIES OF ELECTROSTATIC AND MAGNETOSTATIC ACTIVE SPACE RADIATION SHIELDING

Trac K. Nguyen
Old Dominion University, 2012
Director: Dr. Ravindra Joshi

Developing successful and optimal solutions for mitigating the hazards of radiation in deep space is critical for the success of deep-space long duration explorations, including mission to the Moon, Mars and beyond. A recent report (Tripathi et al., 2008) had explored the feasibility of using electrostatic shielding in conjunction with state-of-the-art materials shielding technologies.

In this thesis research, we study the active electrostatic shielding strategy and examine a hybrid configuration that utilizes both electrostatic and magnetostatic fields. The main advantages of this system are shown to be: (i) much lower magnetic fields that could be below the thresholds set for health and safety for long-term exposures, (ii) a much better shielding and repulsion of incident ions from both solar particle events (SPEs) and galactic cosmic rays (GCRs), and (iii) reductions in the power requirement for re-charging the electrostatic sub-system.

Furthermore, our results show that SPEs radiation can be almost eliminated by these electrostatic configurations. It is also shown that the power needed to replenish the electrostatic charges due to particle strikes from the GCR and SPE radiation is minimal and insignificant.

ACKNOWLEDGMENTS

I would like to first thank all my family members who have been always very supportive and have helped me overcome all the obstacles I faced during my life. I would like to express my gratitude and many thanks to Dr. Ravindra P. Joshi for his support and help throughout this research and my graduate career. His willingness to guide and assist me within this research was impeccable. I would like to thank Dr. Linda Vahala and Dr. Makhin Thitsa for serving on my thesis committee. In addition, I also would like to thank all the faculty members, student advisors, and secretaries at the ECE department.

Finally, thanks are also due to all my friends for their support and advice.

TABLE OF CONTENTS

Page

LIST OF TABLES

LIST OF FIGURES

CHAPTER 1

INTRODUCTION

1.1 Introduction

There is growing interest in a possible manned mission to Mars within various space agencies worldwide including the National Aeronautics and Space Administration (NASA). However, the health risks of space radiation are arguably the most serious challenge to space exploration, possibly preventing these missions due to safety concerns or increasing their costs to amounts beyond what would be acceptable. Radiation in space is substantially different from Earth: high-energy charged particles provide the main contribution to the equivalent dose in deep space, whereas γ rays and low-energy α-particles are major contributors on Earth. This difference causes a high uncertainty on the estimated radiation health risk (including cancer and non-cancer effects), and makes protection extremely difficult. Estimates obtained as early as the 1970s of the mass of radiation shielding required for a crew during interplanetary space flight have shown that the radiation hazard defines, to a great extent, the choice of flight trajectory, launch date, spacecraft configuration, and types of propulsion [1].

Developing successful and optimal solutions to mitigating the hazards of severe radiation in deep space long duration missions is critical for the success these missions, including the Moon, Mars and beyond. Space crews traveling aboard interplanetary spacecraft will be exposed to a constant flux of galactic cosmic rays (GCRs), as well as intense fluxes of charged particles during solar particle events (SPEs). Unlike astronauts serving aboard the International Space Station (ISS), space crews aboard interplanetary

spacecraft (such as the mission of Mars envisioned by NASA) would not be protected by the Earth's magnetosphere. In addition, crews would be exposed to the radiation environment of interplanetary space for extended periods of time. Estimated transit times for a human mission to Mars vary from 100 to 150 days each way with a possible extended duration stay on Mars estimated to be 200 days [2].

In this chapter, the main issues in radiation shielding are briefly outlined. The research problem in the present context is defined, and the central tasks that arise are given. The next section discusses the scope of this thesis research more fully, while the overall outline of this thesis write-up and the subject-matter in the various chapters is given in a subsequent section.

1.2 Thesis Scope and Problem Definition

A strong focus on the safety of the missions and the crew for long duration space missions has begun to emerge as a critical component of planning and design. Hence, shielding of the spacecraft becomes an important issue. In principle, in order to provide shielding, both passive and active strategies can be used. Of these, passive shielding refers to the use of materials having a high atomic mass such as lead to stop or reduce the penetration of the incoming radiation flux. Active shielding, on the other hand, refers to the use of energy-driven devices (such as currents in superconducting magnetic rings, or special structured electrostatically charged to high voltages) to repel the incident ionic flux from the radiation. Of these, passive shielding is the more conventional strategy, and has been studied for over 50 years. Based on such conventional radiation shielding strategies, estimates predict that an interplanetary spacecraft would require substantial shielding of about 50 g/cm^2 of aluminum [3] if the 50 milli-Sieverts (mSv) limit for

astronaut exposure is to not be exceeded. Though other materials (including carbon nanotube-based shielding) might reduce the weight somewhat, these passive shielding strategies are relatively bulky and amount to adding ''dead mass'' to a spacecraft which is not an economically viable solution.

In passive shielding, the energy of the incoming particles is dissipated by multiple collisions within the material. As a result, the effectiveness of a material shield decreases severely with increasing energy of the incoming ions. Since thicker shields have a weight and cost premium, attempting to go with thick passive-shielding is not an attractive or viable path. For example, about 20-30 g/cm^2 of Aluminum material might be needed for a passive shield against SPEs. Also, with passive shielding, the lighter elements provide more effective shielding per unit mass than heavier ones for space radiation environment. Solid material shields cannot be constructed from hydrogen, and from a practical standpoint, carbon appears to offer some relative advantages. In this context, carbon nanotubes, and boron nitride nanotubes are promising. However, one of the disadvantages of passive shielding is the production of energetic high-energy secondary radiation particles (including neutrons) upon the interaction of the incoming ionic flux with the nuclei of the shielding material. These neutrons penetrate deeply can pose serious health risks. Furthermore, the bulkiness and large weight necessary for such passive shields becomes an added liability and burden.

Consequently, more revolutionary technological concepts for space radiation shielding based on active shielding begin to take on added significance and importance. Current conventional radiation protection strategies based on materials shielding alone, have been worked on for about three decades. Any progress using the materials radiation

shielding would only be evolutionary (incremental) at best. Besides, one of the disadvantages of passive shielding is the production of energetic high-energy secondary radiation (including hazardous of neutrons radiation). Furthermore, the bulkiness and large weight necessary for such passive shields becomes an added burden.

Active shielding from ionizing radiation, works by deflecting charged particles outside the protected volume using electromagnetic fields arranged in a suitable configuration. A schematic showing this concept is given in Fig. 1-1.

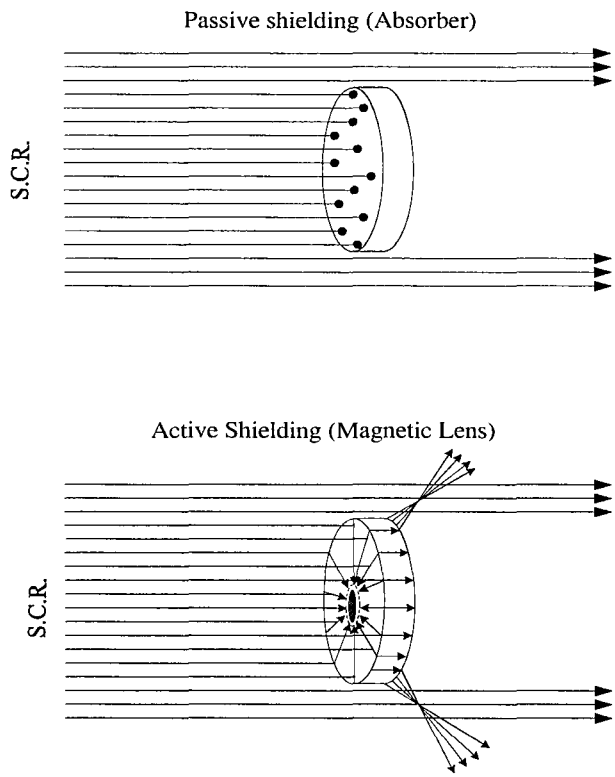

Fig. 1-1. Conceptual difference between passive and active shielding (After Ref. [12]).

Since the early sixties, investigations on the feasibility of active methods, such as electromagnetic fields or plasmas, for shielding spacecraft from hazardous space

radiation have been undertaken with the intention of reducing the mass penalties associated with the use of bulk material shielding in manned spacecraft. These active concepts included the use of electrostatic fields [4], plasmas [5], confined magnetic fields [6] and unconfined magnetic fields [7]. The major focus of the proposed methods was shielding against electrons and protons. Later on, consideration was also given to active shielding against the high-energy heavy ions present in galactic cosmic rays [8]. A comprehensive listing of nearly all publications concerning spacecraft active shielding can be found in Sussingham et al. [9]. A short review of the field was given by Townsend [10].

Townsend [10] demonstrated that electrostatic shields are unsuitable for Galactic Cosmic Rays (GCRs) as well as for Solar Energetic Particles (SEPs) emitted in Solar Energetic Events (SEE). This was because the required electrostatic potentials exceed the current state of the art by over an order of magnitude. Furthermore, electrical breakdown considerations limit the minimum size of the shield configuration to dimensions of the order of hundreds of meters. This latter aspect would make the shields rather bulky.

Among them "Magnetic Shielding" might appear to be a possibility [11] to deflect particles from a region surrounding the spacecraft. However, there seem to be some serious drawbacks to this technology. For this reason, here we would like to make the case in favor of the alternate Electrostatic Active Shielding. Some disadvantages of magnetic shielding include:

(i) Requirements of large currents to produce magnetic fields of ~20 Tesla (T) [12]. However, this requires large currents to produce this range of magnetic field.

Current technological limitations on the achievable currents can yield magnetic fields that are roughly an order-of-magnitude smaller. This is in spite of using high temperature (T_c) superconductor materials. Given this limitation with the current state-of-the art, magnetic shielding cannot be touted as a quick and easy route to success for active shielding.

(ii) Another technological issue concerns the power needed for such systems. Specifically, even if superconducting systems could be used for the currents needed to generate the required magnetic fields in a relatively "lossless" manner, a large amount of power would be demanded by the cryo-cooling system. This would be considered critical during the cool down phase, and also during the "ramp-up" of the magnet. The mass of the cryogenic material and cryogenic system (in addition to any protection system that may be necessary), would also add to the cost of this approach.

(iii) Another problem with magnetic shielding using currents driven through superconducting coils is the adverse effect of magnetic fields on biological tissues [13-15]. For example, magnetic fields may set up damaging currents within blood vessels, as preliminary data seems to suggest [13]. Very simply, blood contains hemoglobin which contains iron (Fe). Since iron is a ferromagnetic substance, it can be affected by strong external magnetic fields.

The circulating blood system can be viewed as fluid confined in space that is transporting ions and charge carriers through. These ions (e.g., sodium, potassium, calcium etc.) are free to move in the blood, but are obviously confined within a specific capillary volume. In the presence of an external magnetic field, a

resonance effect can result in which the ionic currents grow stronger. The strength of the resonance depends on the size of the capillary and the strength of the field. Kanokov et al. [16] suggest that this kind of resonance can occur in the aorta at magnetic field strengths of a few pico-Tesla ($=10^{-12}$ T) and in narrower capillaries at a few hundred micro-Tesla (μT).

Moreover, the flow of blood in the presence of a magnetic field can give rise to induced voltages in the major arteries of the central circulatory system. Studies on rats have shown that magnetic fields can cause significantly increased leakage of their blood albumin through the blood-brain barrier (BBB). Other unwanted and toxic molecules in the blood were also seen to leak into the brain tissue and concentrate in and damage the neurons and glial cells of the brain [17].

Hence, the use of magnetic shielding as a standalone technology for human safety might come at a price. In fact, by creating its own health-related issues, this technology may be creating different kinds of problems from the standpoint of health and safety.

Another issue that must be considered in the active shielding process is the presence of plasmas in space, and any potential effects that a shielding system may (or may not) have on such plasmas. The fields produced by a magnetic-shielding system for deflecting ions would not really steer any plasma that might be surrounding the spacecraft away. Instead, the magnetic fields would give rise to circulating plasma currents. Hence, anyone venturing out of the "protected" space-craft environment would still have to contend with the plasma source outside.

None of these issues exist for electrostatic shielding. On the contrary, electrostatic shielding dramatically reduces biological risks compared to passive material radiation shielding. So given this, the use of electrostatic shielding seems to be an attractive option for deep-space flights. In this context of revolutionary technology for space radiation shielding, detailed analysis was recently presented for a new configuration of electrostatic active shielding [18]. Relevant comparisons were also made with the state-of-the-art passive shielding material. However, there is a need to lower the requisite electrostatic potential for the active shielding, and to further improve upon such active shielding strategies. For example, by reducing the electrostatic potential, the energy requirement for powering up the system could be lowered. For a similar reason, any power expended in re-charging the electrostatic structure due to ionized particle strikes would be reduced if the electrostatic potential were smaller. Finally, electric field thresholds of $\sim 10^4$ V/m have been established from the standpoint of safety for very low frequency electrical excitations [19], and could be a rough limiting estimate for electrostatic charging.

Though the magnetic and electrostatic shielding approaches appear to have advantages over the traditional passive shielding, the technological feasibility of achieving a more optimized result in terms of alternate configurations needs to be investigated. In addition, the use of a single technology alone (whether electrostatic or magnetostatic) could have some serious drawbacks. For example, shields which rely strictly on static magnetic fields to deflect charged particles via the Lorentz force, generally utilize current carrying wires (or coils) that are located at large distances from the spacecraft. However, with these configurations, though the amount of electrical current needed to sustain a given magnetic dipole moment decreases with the coil size,

the shielding capacity is also reduced significantly to the extent that almost no shielding occurs in a region near the center of the coil [20]. On the other hand, if the coils were to be located in close proximity to the spacecraft living for better shielding, then the magnetic field-strengths necessary for protection against GCR particles would be well above 10 Tesla [21].

In the best case scenario, perhaps a combination of the electrostatic and magnetostatic shielding might present a far superior alternative from the standpoint of radiation protection. A coupled, dual-approach could conceivable lower the field requirements, and thus be a safer alternative. The lower field intensities would have the added advantage of reduced power requirements.

The primary goals of this thesis research, therefore, are the following:

(i) Develop appropriate mathematical models that can be used to simulate the dynamics of the incident radiation in outer space. This will require the inclusion of spectra for both Solar Particle Events (SPEs) and Galactic Cosmic Rays (GCRs).

(ii) Study the role of electrostatic shielding and the extent to which it can be used to stop or deflect the incident radiation. At least 2 different electrostatic configurations will be used. One would be a 12-sphere configuration proposed by Tripathi et al. [18] to serve as a baseline for comparisons. A second would be toroidal rings that might have superior shielding characteristics. Other variations and/or combinations will also be probed.

(iii) Implement numerical codes that can track the evolution of SPE and GCR particle trajectories for the electrostatic configurations chosen.

(iv) Evaluate the effectiveness of a hybrid approach that combines both the electrostatic and magnetostatic aspects. Specifically, a combined configuration that uses twelve electrostatic spheres in concert with a current-carrying superconducting ring for a superimposed magnetic field, will be studied.

(v) Effectiveness of shielding, the particle penetration probabilities, and the possibility of charging/discharging the electrostatic structures will also be studied as a function of incident energy, as part of this thesis research. Other aspects such as the voltage dependence and role of the dimensions will be probed.

1.3 Summary

This thesis research centers on a simulation study of active radiation shielding. The electrostatic approach is the primary focus. However, in addition, a hybrid scheme involving both magnetostatic and electrostatic fields will be probed. This is primarily driven by the needs within NASA and other aerospace agencies worldwide to develop a comprehensive, economic and effective shielding strategy.

In chapter 2, a literature review and background information on the state-of-the-art will be presented and discussed. Next, in chapter 3, the model and numerical simulation technique used for this thesis research will be discussed in detail. This will be followed by a presentation of the results obtained. The significance and implication of the results will be discussed in chapter 4. Finally, a summary of this research finding, the

salient conclusions and potential implications will be given in chapter 5. In addition, possibilities for future work in this area will also be outlined in chapter 5 for completeness.

CHAPTER 2

BACKGROUND AND LITERATURE REVIEW

2.1 Introduction

The radiation in space is from three sources consisting of every known particle including energetic ions formed from stripping the electrons from all of the natural elements. The three sources of radiation are associated with different origins identified as those of galactic origin (Galactic Cosmic Rays, GCRs), particles produced by the acceleration of solar plasma by strong electromotive forces in the solar surface and acceleration across the transition shock boundary of propagating coronal mass ejections (solar energetic particles, i.e., SEPs), and particles trapped within the confines of the geomagnetic field. The GCR constitutes a low level background which is time invariant outside the solar system but can be modulated over the solar cycle. The SEP is associated with some solar flares which produce an intense burst of high energy plasma. The trapped radiation consists mainly of protons and electrons within two bands centered on the geomagnetic equator between Low Earth Orbit (LEO) to interplanetary space. However, the most concerning of the radiation in space are the SEP and the GCR.

Astronaut exposure to galactic cosmic rays (GCRs) and solar particle events (SPEs) is an important safety concern for space exploration. Radiation risks include carcinogenesis, degenerative tissue effects such as cataracts [22] or heart diseases [23, 24], and acute radiation syndromes [25]. Other risks such as damage to the central nervous system (CNS) are a potential concern for the GCR heavy ions [26]. In the past, career radiation limits have been based on fatal cancer risks. For low Earth orbit (LEO) programs, an excess 3% risk of a fatal cancer is used as criteria for dose limits, which are

applied using age and gender specific dose to risk conversion factors. Radiation risk projection models serve several roles, which include setting dose-to-risk conversion factors needed to set dose limits, projecting mission risks, and evaluating the effectiveness of shielding or other countermeasures.

In the usual context, shielding implies an alteration of the radiation through interactions with intervening materials by which the intensity is decreased. Alternate techniques that rely on deflecting the incoming ionized particles (known as active shielding) may also be used. In this chapter, some of the strategies for shielding will be reviewed. The possible biological effects of radiation for long-duration space flights will also be discussed. Based on the literature review, a case can be made for the use of electrostatic or (even better) perhaps even a hybrid (electrostatic-cum-magnetostatic) shielding scheme. These radiation shielding approaches will then be taken up for analyses and numerical evaluation in subsequent chapters of this thesis research.

2.2 Origin and Types of the Space Radiation

The harsh conditions considered in space include energetic particle radiation, plasmas, absence of air (especially in human spaceflights) and debris, all of which pose severe challenges for astronauts and precision payloads. The space radiation environment is distinct from the others and deserves special attention. The radiation environment, consisting of trapped radiation belts in the Van Allen belts, albedo particles (mostly neutrons) produced by scattering of primary radiation from Earth's atmosphere, galactic cosmic rays, and solar energetic particles, leads to effects such as radiation damage, single-event upsets in electronics, background in detectors, and health hazards to astronauts in human spaceflights. In interplanetary space, the radiation environment

mainly consists of two sources: the galactic cosmic rays originating from outside of the solar system and the solar energetic particles. These particles are associated with the acceleration of coronal mass ejection (CME) [27] and possible acceleration in the solar surface due to a large disturbance [28]. The intensity of both components (SPE and GCR) depends on the level of solar activity. However, this dependence for GCR and SPE fluxes is opposite: at high solar activity GCR fluxes are relatively small, whereas the probability of SPE flux appearance is high; during low solar activity periods the situation is inverse.

The extreme value of the solar energetic particle fluencies is certainly one of the factors limiting the diversity of human activity in space. More information relating to SPE distributions and characteristics can be obtained by gathering data from satellites. There has been much activity in this regard over the past 20 years, and numerous models of SPE have been constructed. The three best-known models for solar particles are those by Nymmik [29, 30], Xapsos et al. [31] and Feynman et al. [32]. Based on measurements, the model probability of the SPE flux is as shown in Fig. 2-1. In spite of the variety of prior analyses of solar proton events, no general procedure has emerged for describing the complete distribution of event magnitudes, either for event fluencies or for peak fluxes. Thus far, only empirical approaches have been used, and all of these give a reasonable description of only a limited portion of the probability distribution. For example, lognormal distributions [33, 34] and power law distributions [35] have been used. From a more general viewpoint, the basic difficulty with describing solar proton event distributions arises from the incomplete nature of the data. Extremely large events occur very infrequently. For example, since the earliest reported peak flux values of

1967, only 3 separate events have produced five minute averages of > 10 MeV flux that exceed 10^4 $cm^{-2}s^{-1}sr^{-1}$[36]. Such events are the most important from a radiation effects viewpoint, yet statistically are the least well characterized. SPEs are unpredictable, develop rapidly, and generally last for no more than some hours; however, some proton events may continue more than several days. In a worst case scenario, the emitted particles can reach energies up to several Gigaelectron-volt (GeV) per atomic mass unit, and doses received could be immediately lethal for an astronaut in free space.

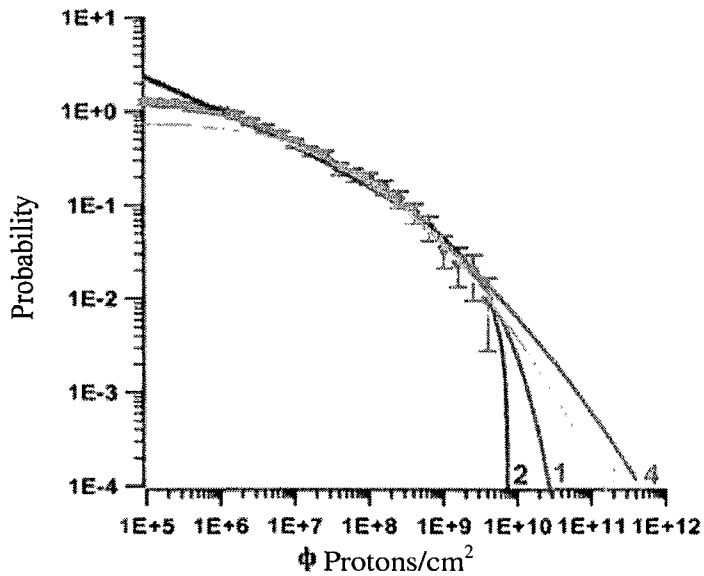

Fig. 2-1. Probability of the SPE flux based on the following four models: (1) The studies of Nymmik [30], (2) the model by Xapsos [31], (3) the Feynman model [32], and (4) best fit to experimental data available as of 2011 (After Ref. [30,31, and 32]).

Galactic cosmic rays (GCRs) are cosmic rays that have their origin inside our galaxy, outside our solar system. GCRs are high-energy charged particles, and are usually protons, electrons, and fully ionized nuclei of light elements. The advanced composition explorer (ACE) of NASA launched in 1997 has been in orbit for many

years. Several high-resolution spectrometers onboard the ACE have measured the elemental, isotopic, and ionic charge state composition of nuclei from H to Ni ($1 \leq Z \leq 28$) from solar wind energies of ~1 keV/nucleon to galactic cosmic ray (GCR) energies of ~500MeV/nucleon [37]. Most cosmic rays are the nuclei of atoms, ranging from the lightest to the heaviest elements in the periodic table. Cosmic rays also include high energy electrons, positrons, and other subatomic particles. About 89% of the nuclei are hydrogen (protons), 10% helium, and about 1% heavier elements [38]. The common heavier elements (such as carbon, oxygen, magnesium, silicon, and iron) are present in about the same relative abundances as in the solar system, but there are important differences in elemental and isotopic composition that provide information on the origin and history of galactic cosmic rays. For example there is a significant overabundance of the rare elements Li, Be, and B produced when heavier cosmic rays such as carbon, nitrogen, and oxygen fragment into lighter nuclei during collisions with the interstellar gas. Electrons constitute about 1% of galactic cosmic rays. Their kinetic energies extending beyond 10^{20} eV [39] are thought to be of galactic origin with sources like supernova explosions of massive stars. Energies above 10^{18} eV are thought to have extra-galactic origin [40]. The energy range of GCR extends over more than 15 orders of magnitude from less than 1 MeV (=10^6 eV) to more than 10^{21} eV. When GCR enters our Solar System, it has to overcome the outward-flowing solar wind, the intensity of which varies according to an approximately 11-year cycle of solar activity. Hence, the GCR fluxes also vary with the solar cycle, an effect known as solar modulation. Differences between solar minimum and solar maximum are a factor of approximately five. At peak energies of about 200–700 MeV/unit during solar minimum, particle fluxes (flow rates)

reach 2×10^3 protons μm^{-2} $year^{-1}$ and 0.6 Fe-ions μm^{-2} $year^{-1}$. As dose to an individual cell is proportional to the square of the particle's energy dependent effective charge [41], the iron ions contribute nevertheless significantly to the total radiation dose. Typical radiation sources in our solar system are shown in Fig. 2-2. Some of the models that have been developed and frequently used in the space dosimetry literature are those of Tylka et al. [42] and Badhwar-O'Neill [43]. These models have the capability of describing spectra of GCR nuclei between $1 \leq Z \leq 26$ over an energy range from 10 to 10^5 MeV/nucleon.

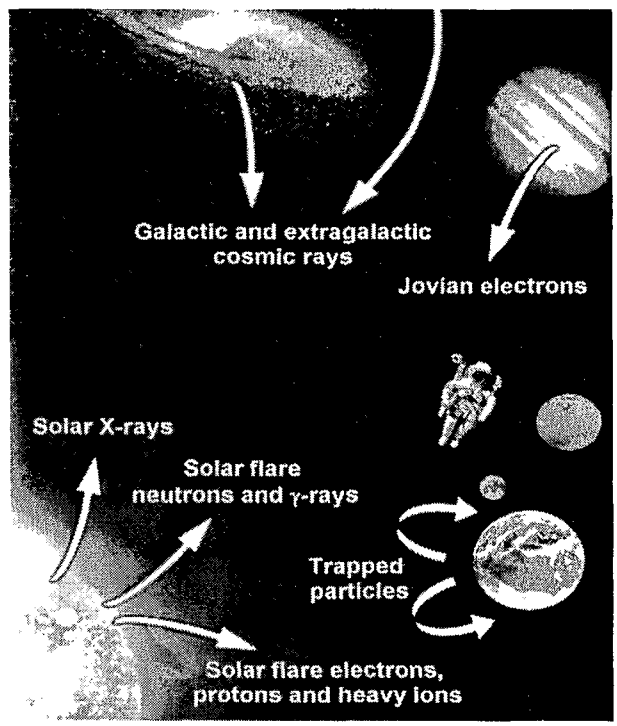

Fig. 2-2. Space radiation sources of our solar system. Of special concern for long-duration space missions are GCR, electrons, protons and heavy ions of SPE (After Ref. [46]).

2.3 Shielding Strategies for the Lunar Environment

Unlike Earth, the Moon does not have a magnetic field to deflect or trap galactic cosmic rays (GCRs). On the other hand, solar particle events (SPEs) surface exposures are only about half those experienced in deep space due to the shadowing provided by the Moon itself [44]. The skin shell concepts currently proposed for NASA's Crew Exploration Vehicle (CEV) design [45] consisting of 5.0–7.0 mm thick aluminum is expected to be adequate for GCR protection over short- duration surface missions. This would be expected to keep the dose exposures below a designated 500 mili Gray (mGy) – the equivalent of radiation annual limit.

A variety of accommodations for a crew of four have been proposed under lunar conditions. These include storm shelters (from solar flares and SPE activity), and deployable and movable sleep and radiation shelter schemes. Some of concepts [46] are shown in Fig. 2-3 and 2-4. Deployable drop-down sleeping units with water tube radiation shielding can utilize potable and wastewater in separate tubular piping systems.

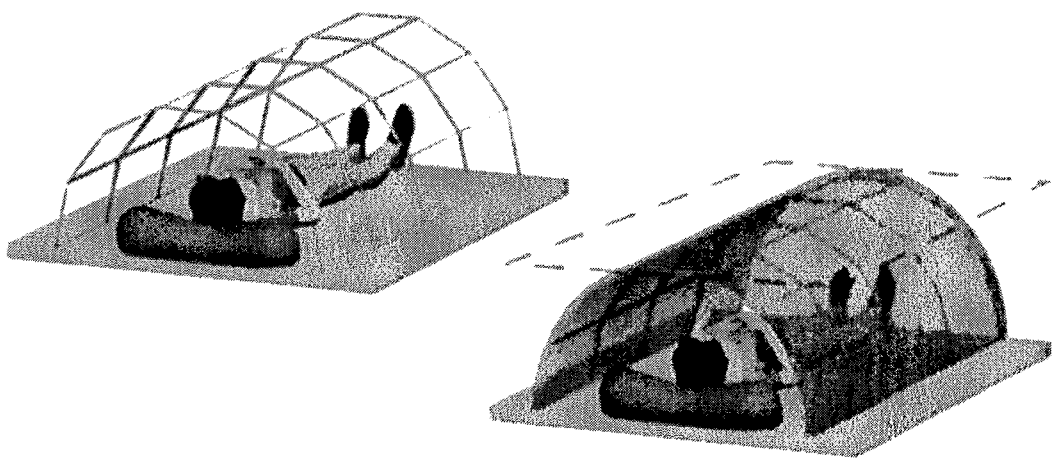

Fig. 2-3. Single-person storable/reloadable radiation shielded sleep unit (After Ref. [46]).

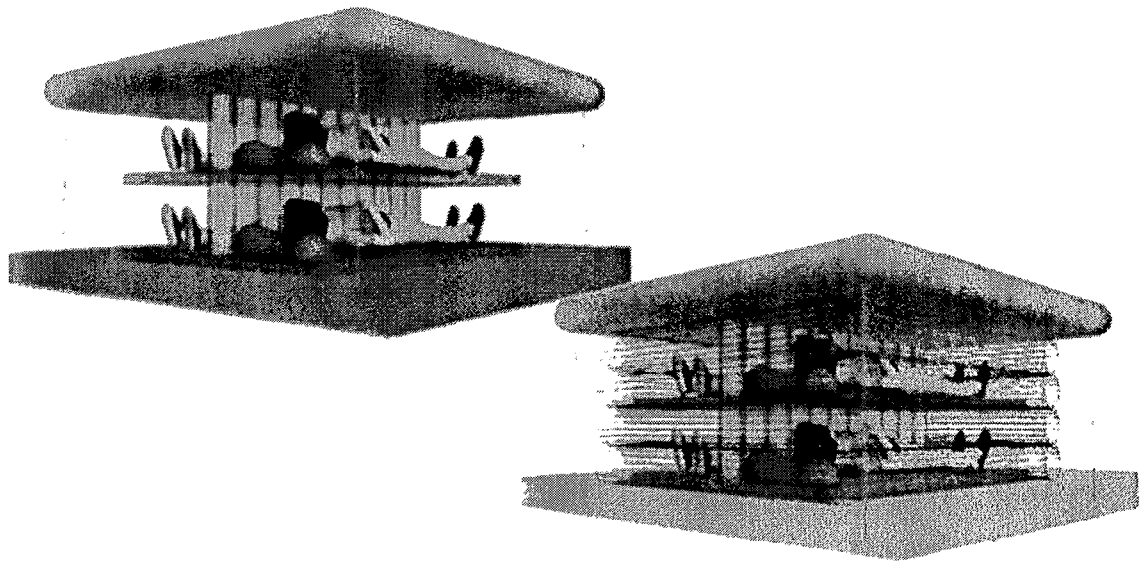

Fig. 2-4. Deployable drop-down sleeping units with water tube radiation shielding (After Ref. [46]).

Water supply for these systems can conceptually be located above the ceiling (as shown in Fig. 2-), and heights of the sleeping units might be kept to a minimum in order to reduce water requirements. For a four-person sleeper in Fig. 2-4, the lengths and widths could be on the order of 2 meters and 1.5 meters, respectively. However, for deep space mission, the high-energy GCR radiation is a primary concern (rather than SPE which has lower particles energies), the simple deployable and movable sleep and radiation shelter schemes will not be sufficient for the radiation shielding. Revolutionary active shielding or hybrid strategies would be required. These aspects are discussed in the next section.

2.4 Radiation as a Risk Factor for Humans

Radiation risk as a factor for humans in space falls in two categories: i) it can nearly immediately affect the probability for successful mission completion (mission criticality), and ii) it can result in radiation late effects in the individual space traveler. In

both cases, risk is considered to be a monotonic, increasing function of dose and, thereby, correlated to space environmental parameters and mission duration. Up to now, manned missions outside the shield provided by the Earth's geomagnetic field were limited to the short visits of the lunar surface by the Apollo crews. Fortunately during these excursions the normal, 'steady' state of the cosmic radiation field prevailed, thereby the Apollo crews were spared to exposure to higher fluxes of SPEs. Long-term manned missions started with the Skylab crews were extended by the Mir cosmonauts and will further expand during the utilization of the International Space Station (ISS).

From the standpoint of health and safety of the space-crew, quantitative estimates of the biologically effective radiation doses and the radiobiological effects on humans and impact on the performance and life expectancy have to be developed. Early health effects from acute irradiation have the potential to degrade crew performance and, hence, to interfere with mission success, whereas late effects will not ensue until years, sometimes decades, after completion of the mission. A well-known late effect from space radiation with higher doses is the induction of lens opacities [47]. The threshold for detectable cataract formation is about 2 Sieverts (Sv) for acute sparsely ionizing radiation doses and 15 Sieverts (Sv) for protracted doses. For example, the astronauts of the Apollo 11 mission, returning from the Moon, reported light flashes, i.e. faint spots and flashes of light at a frequency of one or two per minute after some period of dark adaptation. Evidently, these light flashes result from high energy particles of cosmic radiation penetrating the spacecraft structure and the astronaut's eyes and producing visual sensations through interaction with the retina.

Fatal neoplasm of the blood forming organs (BFOs) give rise to one of the most frequent radiogenic cancer, i.e., leukemia, which in addition, has the smallest latency times of radiogenic cancers of the adult. The development of a tumor as a radiation late effect is still poorly understood, but it is clear that many stages are involved. The first stage, induction or initiation, can definitely be caused by radiation, although its role in promotion and progression is not yet clear. The development of a tumor as a radiation late effect is still poorly understood, but it is clear that many stages are involved. The first stage, induction or initiation, can definitely be caused by radiation, although its role in promotion and progression is not yet clear. NASA currently does not accept higher than a 3% risk of a fatal cancer over the lifetime of an astronaut. For the particles composing space radiation, energy deposition is highly localized along the trajectory of each particle. High-energy charged particles lose energy when they traverse any material, even the human body. GCR particles of average energy can penetrate a substantial thickness of materials, and their lighter secondary products will be able to penetrate even further. For this reason, the biological effectiveness of radiation will change as a function of depth of penetration. A broad spectrum DNA lesion is also induced as a result of exposure to ionizing radiation [48].

Tables 1, and 2 give the radiation equivalent doses [49] for the skin, the ocular lens, and blood forming organs (BFOs).

Tissues	30 days Sievert (Sv)	Annual	Career
Skin	1.5	3.0	6
Ocular lens	1.0	2.0	4
Blood forming organs	0.25	0.5	0.075*(Age-30)+2 (m) 0.075*(Age-38)+2 (f)

Table 1. NASA organ dose limits based on age and gender (m/f) (After Ref. [49])

Shield/thickness	Tissue	Free space equivalent dose Sievert (Sv)	Lunar equivalent dose Sievert (Sv)	Mars equivalent dose Sievert (Sv)
Space suit (0.3 g cm^{-2} Al)	Skin	295.1	147.55	0.45
Space suit (0.3 g cm^{-2} Al)	Ocular lens	81.3	40.65	0.44
Space suit (0.3 g cm^{-2} Al)	Blood forming organs	4.21	2.11	0.32
Pressure vessel (1 g cm^{-2} Al)	Skin	64.4	32.2	0.44
Pressure vessel (1 g cm^{-2} Al)	Ocular lens	35.5	17.75	0.42
Pressure vessel (1 g cm^{-2} Al)	Blood forming organs	3.52	1.76	0.31
Room (5 g cm^{-2} Al)	Skin	6.48	3.24	0.38
Room (5 g cm^{-2} Al)	Ocular lens	5.54	2.77	0.37
Room (5 g cm^{-2} Al)	Blood forming organs	1.93	0.97	0.28
Shelter (10 g cm^{-2} Al)	Skin	2.62	1.31	0.33
Shelter (10 g cm^{-2} Al)	Ocular lens	2.43	1.22	0.32
Shelter (10 g cm^{-2} Al)	Blood forming organs	1.26	0.63	0.25

Table 2. Mission doses from SPE under various conditions (After Ref. [49]).

2.5 Passive Shielding for Deep Space

Unlike the lunar environment where the radiation tends to be dominated by lower energy SPE, deep-space exploration including colonization of Mars will involve shielding against GCR ions. These have much higher energy and mass, and thus are more penetrating. Hence, this issue needs to be addressed. A Moon-base scenario will likely consist of a lunar human outpost on the South Pole with constant sunlight illumination and potential resources of water-ice deposits [49]. Possible plans include a follow-up short-term trip to Mars of about 500 days with a 30-day stay on Mars, or a long-term Mars scenario of about 1,000 days with a 525-day stay on the Mars surface. In this context, a manned mission to Mars offers advantages that automated missions cannot provide. For example, humans can make their own decisions when it comes to acting on data.

First, an overview and discussion of passive shielding is given in this section. The basic idea is to stop incoming ions from penetrating a shield. A simplistic view might be that better shielding can be achieved by having a thicker layer for reduced penetration. However, as the thickness increases, shield effectiveness drops. This is the direct result of the production of a large number of secondary particles, including neutrons, caused by nuclear interactions of the GCR with the shield material. SPE radiation is less of an issue because it does not produce these secondary particles. For example, the outer walls of the spacecraft provide total protection from protons up to a 50–70 MeV when about 5 g/cm^2 of material is used for shielding. However, during some exceptionally intense solar events, a great number of protons are ejected at higher energies. In this case, the dose released in a few hours can exceed the dose limits

recommended for astronauts' protection, and lead to acute, deterministic effects, including lethal radiation syndromes.

Immense work has already been done in developing passive shielding strategies for human space exploration missions, mostly performed by NASA researchers [50, 51]. This activity resulted in numerous workshops and publications in this area. All calculations and measurements show that light, highly hydrogenated materials (such as polyethylene) are ideal materials for space radiation shielding [52, 53]. Bulk shielding poses obvious weight problems on the spacecraft. A heavy load, added purely for reducing radiation exposure, becomes a substantial mass penalty and may therefore dramatically increase the mission cost.

Currently, NASA uses aluminum for radiation shielding. This material is marginally effective at radiation shielding, since it has a low electron density. Therefore, researchers have been looking for other materials, which have higher hydrogen content than aluminum, to use as radiation shielding materials. Polymers have been a natural area of interest, due to the possibility of creating very good multi-functional materials. Polyethylene is often used along with aluminum as a benchmark for making comparisons about the radiation shielding effectiveness of a new material. Polyethylene is of particular interest because it inherently has the highest hydrogen content possible in a polymer. Furthermore, polyethylene does not contain any large nuclei, which is important because the absence of large nuclei dramatically reduces the risk of the shielding material fragmenting from a collision with a radiation ion. That is beneficial, because it reduces the number of particles that must be dealt with by an effective radiation shield. Unfortunately, polyethylene does not possess particularly good thermal

and mechanical properties, and so it is difficult to use it in the harsh space environment. More recently, new materials such a carbon nanotubes are being tested for possible use.

2.6 Active Shielding for Deep Space

Active shielding eliminates the need for massive shields by using electric or magnetic fields to deflect particles from a region surrounding the spacecraft. However, a different set of issues both technical and practical are presented by these shielding strategies. The most serious is the safety concern due to the exceptionally large voltages (>1 kV) or large magnetic fields (>1 T) in close proximity to the spacecraft occupants that are required to shield the hazardous GCRs.

The main types of active shielding methods that have been proposed and studied are based on either magnetic shielding or electrostatic shielding. For certain magnetic field configurations, the influence these fields impart on charged particles via the Lorentz force can lead to regions of space for which particles below a certain energy are forbidden access. These regions of space are said to be shielded from such particles. Using the concept of a magnetic potential barrier, Stormer first showed the existence of a shielded region for a dipole magnetic field configuration [54]. Specifically, Stormer showed that a toroidal region exists around the center of a dipole magnetic field from which particles of a given energy are excluded.

With regards to magnetic shielding, there have been several ideas for creating the fields necessary for deflection of incoming radiation. One concept is based on plasma magnets. In this scheme, a plasma (ionized gas containing positive ions and/or electrons) surrounds the spacecraft. A rotating magnetic field drives current in the plasma similar to the circular motion of an electric fan. This current then produces a static magnetic field

which can act as the barrier to incoming radiation and deflect both SPE and GCR particles. The required rotating magnetic field can be generated based on a coupled capacitor-inductor circuit as shown below in Fig. 2-5. A conceptual view of such plasma driven magnetic shield is shown in Fig. 2.6. Another possibility is that of using a circular loop of radius "a" that created a shielded region around a spacecraft as shown in Fig. 2-6. Yet another configuration is of using a torus with current carrying wires that surround the spacecraft, sketched in Fig. 2-7. The magnetic fields produced once again could be utilized for deflection. Finally, a double toroidal-solenoid superconducting magnetic shield as shown in Fig. 2-8 was proposed by Hoffman at the Massachusetts Institute of Technology [55].

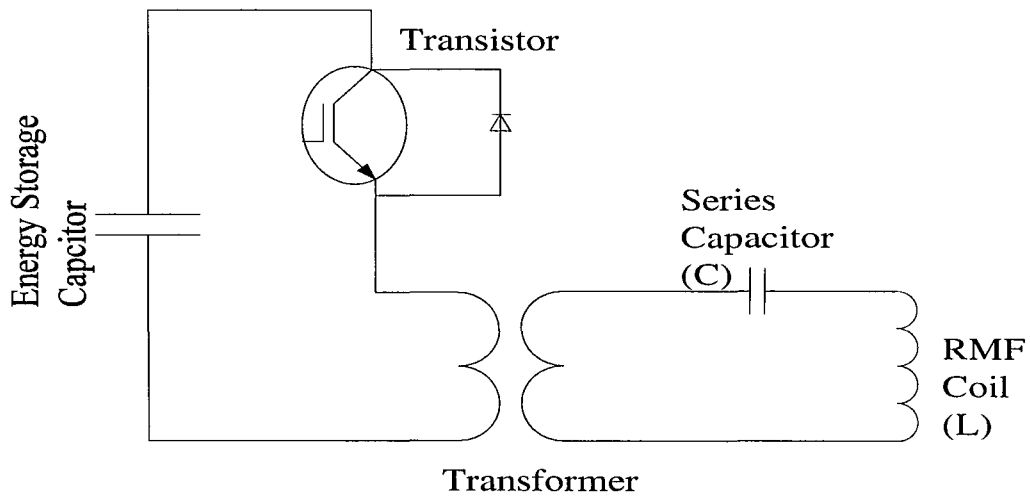

Fig. 2-5. Circuit schematic for obtaining a rotating magnetic field (After Ref. [56]).

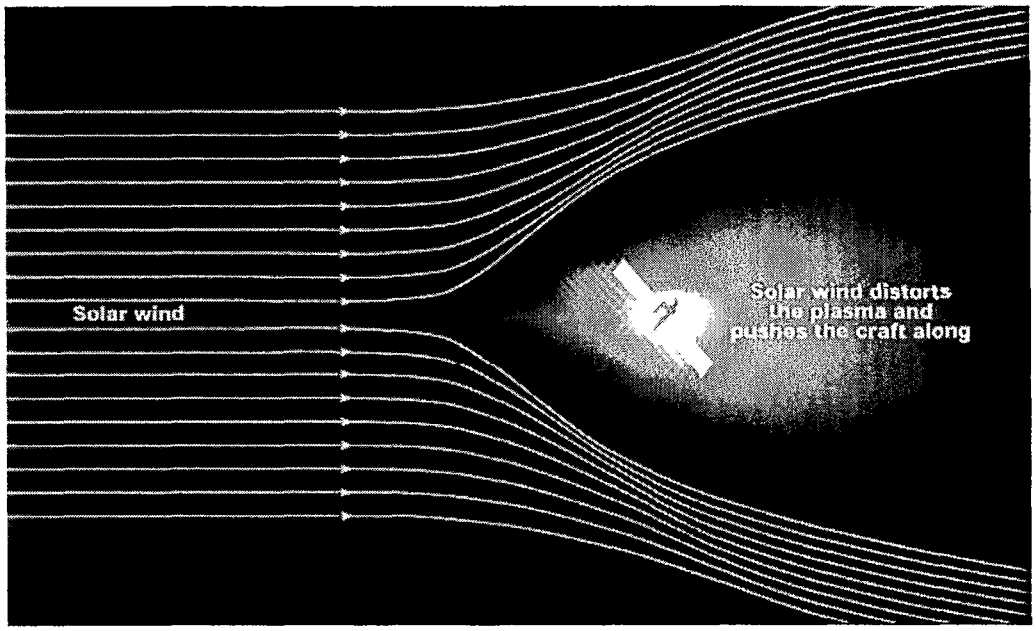

Fig. 2-6. Circuit schematic of magnetic shielding based on deflection (After Ref. [56]).

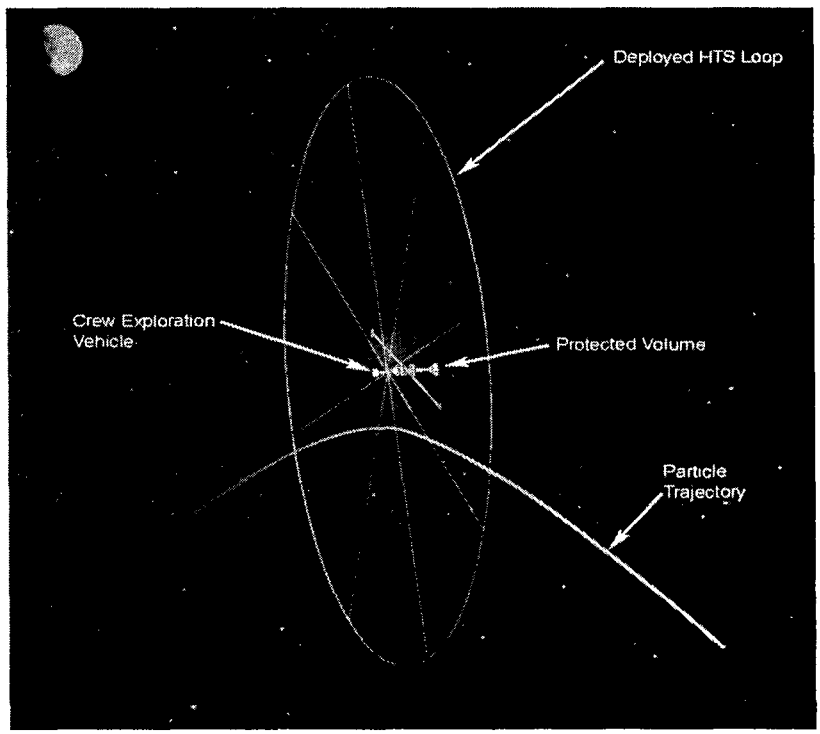

Fig. 2-7. Magnetic shield based on a current carrying wire loop (After Ref. [56]).

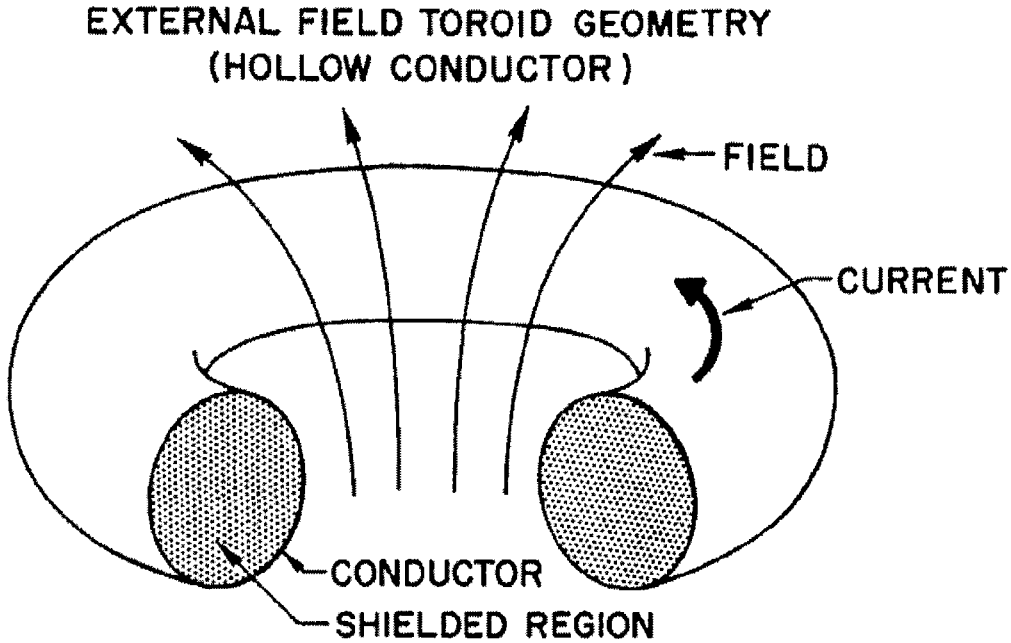

Fig. 2-8. An unconfined magnetic produced by a current carrying loop (After Ref. [6]).

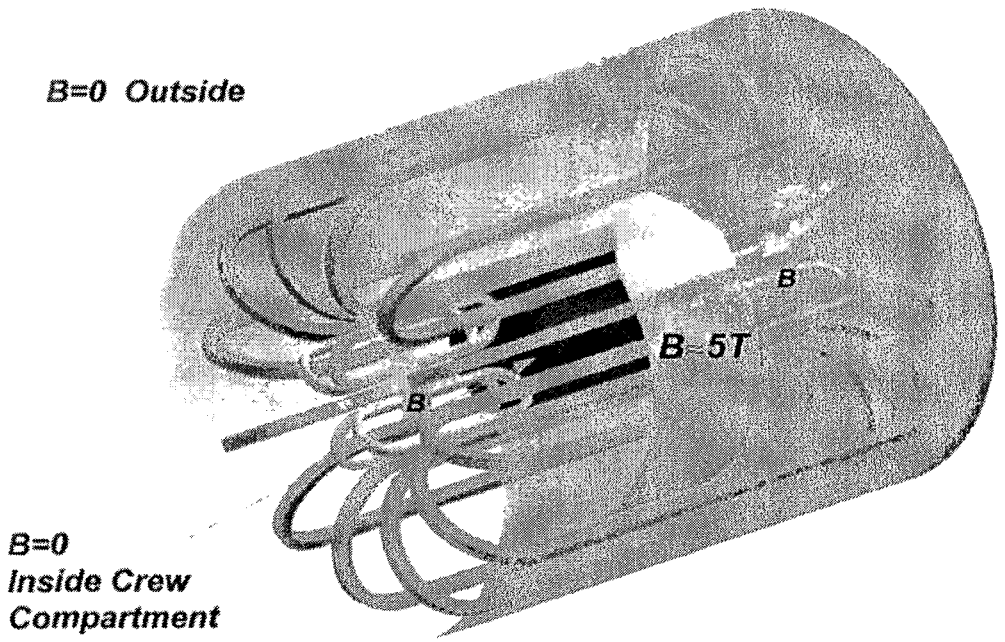

Fig. 2-9. The double toroidal-solenoid superconducting magnetic shield proposed by Hoffman (After Ref. [55]).

Electrostatic shielding is based on charging a given configuration or systems of elements to a large potential. The voltages can be very high in the Mega-Volts range. An example of such a recently proposed configuration is by Tripathi et al. [57], with the proposed geometry shown in Fig 2-10.

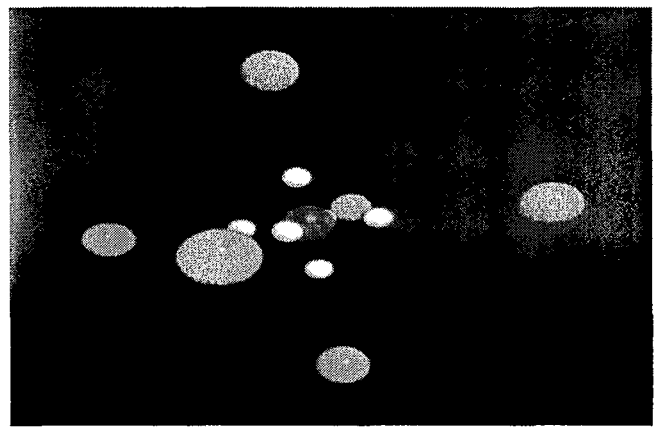

(a)

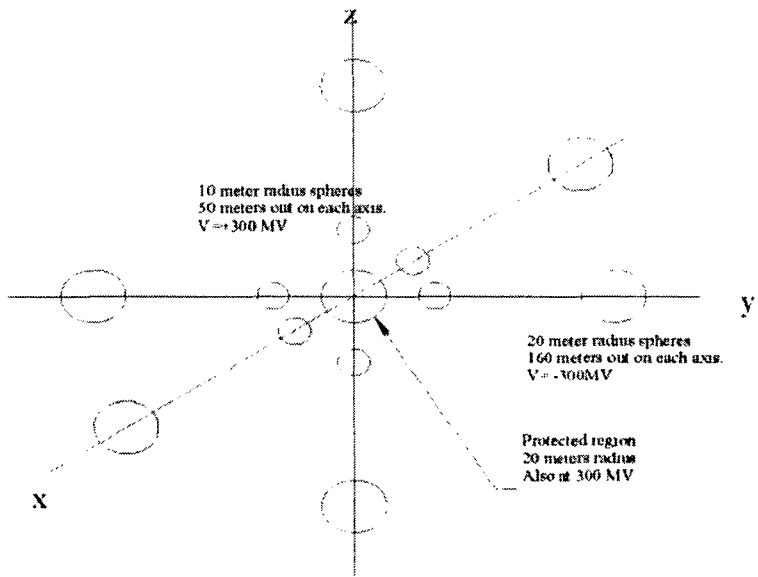

(b)

Fig. 2-10. A proposed electrostatic shielding configuration (After Ref. [57]). (a) A configuration in 3D model, (b) A configuration in 3 coordination model.

In the geometry shown in Fig. 2-10, the overall configuration was composed of a set of 12 spheres, with the center sphere represents a protected region within which is the spacecraft itself. The outer spheres were taken to be 20 m in radius, located 160 m along each axis, and kept at a potential of -300 MV. The inner spheres were 10 m in radius, located 50 m along each axis and are at a potential of +300 MV.

The electrostatic idea can be taken further in order to make it better suited for space applications where light-weight and compactness are important considerations. Thus one could think of using inflatable, mesh structures such as the configuration shown below in Fig. 2-11. In this mesh structure, the grid points denote charged dielectric spheres while the interconnections provide a support structure. Initially such a structure could be in an uncharged and collapsed state. Upon charging the grid points at the time of deployment, mutual repulsion would automatically lead to their separation, and the entire structure would inflate to a final spherical geometry. Such an inflatable, mesh-structure would have numerous advantages. These include: (i) Light weight, (ii) Compactness, (iii) Lower secondary emission due to decreases in the contact surface area and target collisional sites. (iv) Higher charge retention leading to significantly lower steady-state power requirements. (v) Finally, the separation between the individual grid points can be an additional tunable parameter. Increasing the spacing, for example, would reduce leakage currents even further.

The electrostatic shielding concept could be used not just around spacecraft, but also as shelters for extra-terrestrial bases. This is shown conceptually in Fig. 2-12. Due to the inflatable nature of these structures, such shields would mimic "anti-radiation umbrellas" and scaled down versions could even be deployed on space vehicles and

transportation platforms. These light-weight structures could inflate through electrostatic charging.

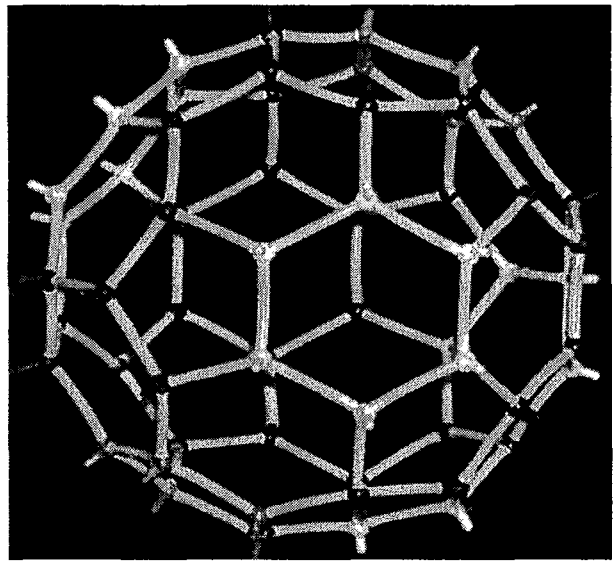

Fig. 2-11. Possible mesh-type geometry for electrostatic shielding (After Ref. [58]).

The biggest advantage of active electrostatic radiation shielding is that by preventing ions from hitting the spacecraft, the unknown harmful biological effects of continuous long duration exposure to space radiation would be significantly reduced (~70 %) for galactic cosmic rays (GCR) and nearly 100% for solar particle events (SPE). It is believed that the best strategy for radiation protection and shielding for long duration human missions is to use electrostatic active radiation shielding while, in concert, taking the full advantage of the state-of-the-art evolutionary passive (material) shielding technologies for the much reduced and weakened radiation that may escape and hit the spacecraft.

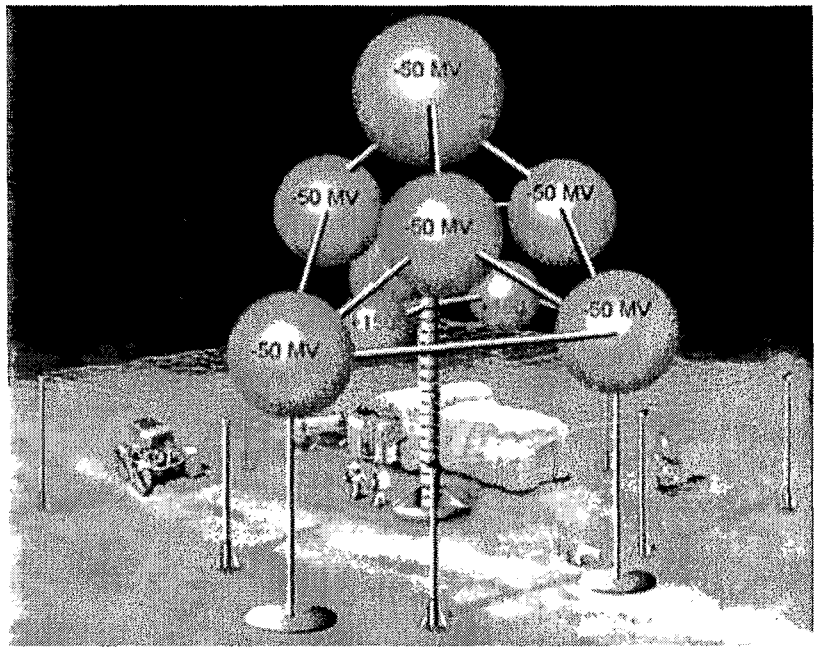

Fig. 2-12. Concept of electrostatic radiation shield on an extra-terrestrial base with negative outer spheres and positive inner spheres (After Ref. [58]).

2.7 Summary

So in conclusion, the demands of deep-space exploration, including possible colonization of the moon and expeditions to Mars place a critically important need on radiation shielding for the health and safety of astronauts. Previous research and development in radiation shielding had primarily relied on passive methods using thick material covers and envelopes. However, in deep space where high energy particles (arising from GCR and SPE) are generally encountered, the passive shielding methods would likely not be very useful. Very thick shields would be needed to counter act the penetrating power of the incident radiation. Given that bulky volumes are unacceptable due to the high costs of building and transporting such large and unwieldy structures in deep space, passive shielding does not appear to be a viable solution. Hence, new

concepts and ideas based on active shielding are required. Electrostatic and magnetic shielding are two of the plausible technologies in this realm. Of these, electrostatic shielding might have an advantage since it does not lead to large magnetic fields that can potentially be dangerous from the standpoint of human exposure. Consequently, here in this thesis work, we will focus primarily on the electrostatic shielding aspect. However, for completeness, a hybrid approach that includes some elements of magnetic shielding will also be evaluated. The next chapter will focus on the underlying theory and equations used for our active shielding analyses. The results obtained from our model implementation will then be presented and discussed in chapter 4.

CHAPTER 3

METHOD OF ANALYSIS

3.1 Introduction

In this chapter the methodology for analyzing the effectiveness of shielding systems against space radiation will be presented. First, the mathematical model and related equations for predicting the trajectories of incident space radiation will be discussed for electrostatic systems. These can be used for any configuration. Such system configurations will all be assumed to be held at some fixed potentials V_i. In a later section, the simulations appropriate for ionized particle deflection by both electrostatic and magnetostatic fields will be discussed. This is finally followed by discussions of the Monte Carlo method for keeping track of the trajectories of incident particles that encounter such shielding systems.

3.2 Forces and Equations of Motion due to Electrostatic Fields for Spheres and Rings

For a given potential configuration, the influence that the electrostatic fields have on incident charged particles via the collective Coulomb forces can lead to regions of space within which particles below some energy are unable to enter. These "forbidden" regions of space are said to be shielded from the incoming particles. A simple example of this concept to the electrostatic case is shown in Fig. 3-1(a) and 3-1(b). The geometries considered for electrostatic shielding in Fig. 3-1(b) consists of six inner positively charged spheres, while the configuration of Fig. 3-1(a) shows three positively

charged toroidal rings. Each of the figures 3-1(a) and 3-1(b) include six negatively charged outer spheres.

The easiest to consider is the simple configuration of a single charged sphere, held at potential V_j and having an associated charge Q_j on the surface. The equation of motion of a particle with charge q_i, moving with velocity v_i in a collective electrostatic field is given by:

$$\gamma m_i \, d\mathbf{v}_i/dt = \sum_j q_i \mathbf{E}_{ij} = \sum_j q_i Q_j (\mathbf{r}_i - \mathbf{r}_j)/[4\pi\varepsilon_0 \, |\mathbf{r}_i - \mathbf{r}_j|^3], \tag{3.1}$$

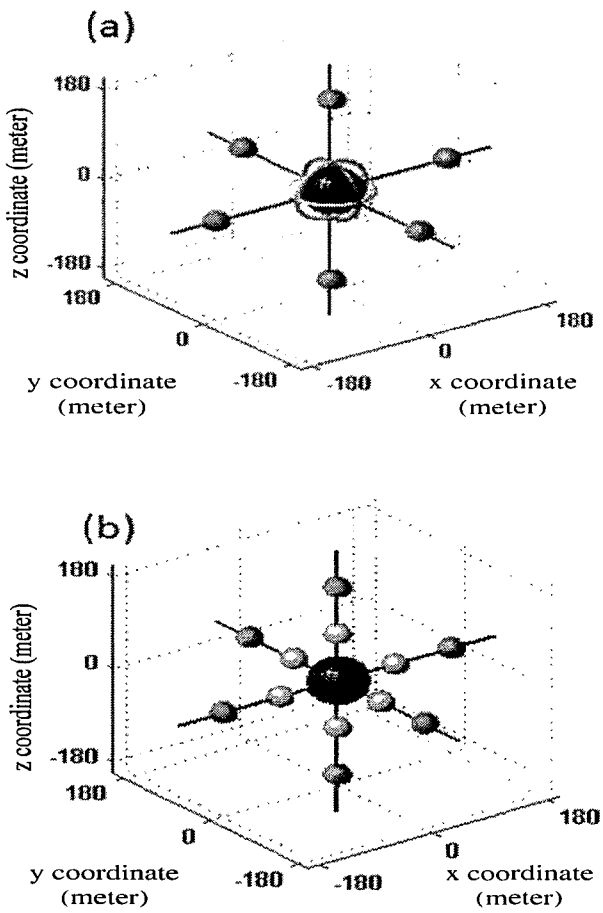

Fig. 3-1. Geometries considered for electrostatic shielding. (a) Three toroidal rings with six negatively charged spheres, and (b) a twelve-sphere with six positive and six negative spheres.

where m_i is the rest mass of the i^{th} particle, $\boldsymbol{r}_i$ and $\boldsymbol{r}_j$ are the position vectors of the incoming particle and the center of the sphere held at a surface potential V_j, respectively.

In the equation (3.1), the summation is over all the charged spheres in the shielding configuration, $\gamma = (1 - |v_i|^2/c^2)^{1/2}$ is the relativistic correction factor, c is the speed of light, ε_0 is the free-space permittivity, and $\mathbf{E}_{ij}$ the electrostatic field at the location of the charge q_i.

The potential and electric field distributions for toroidal rings are somewhat different from those created by charged spheres. The electrostatic shielding here is taken to consist of three doughnut-shaped toroidal rings with axial symmetries along the x-, y- and z-directions. For simplicity, figure 3-2 shows only one ring being considered around the z-axis.

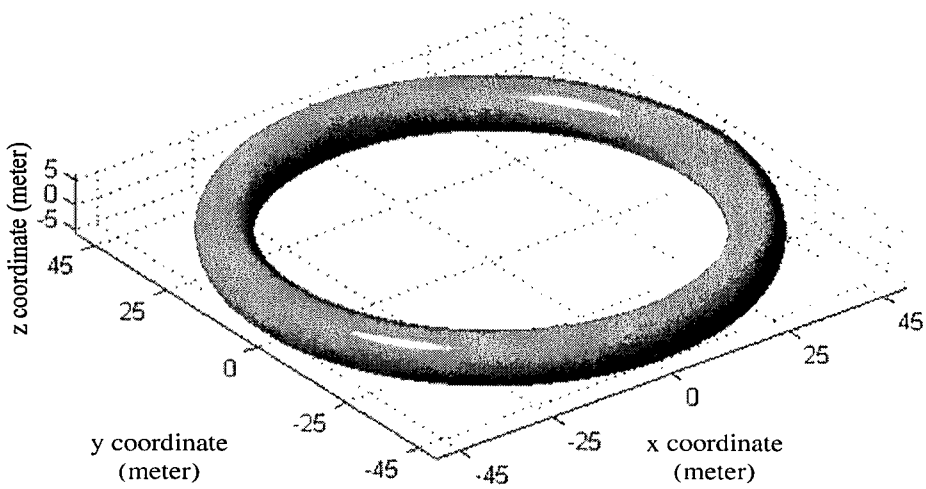

Fig. 3-2. Toroidal ring geometry for simple analysis.

The mean radius of the torus in the z = 0 plane is 45 meters with a thickness of 10 meters. Given the geometry, the toroidal co-ordinate system is best suited for the analyses. Using the notation (ν,u,Φ), the toroidal coordinates are related to the usual Cartesian co-ordinates (x,y,z) as:

$$x = A \sinh(\nu) \cos(\Phi)/[\cosh(\nu) - \cos(u)], \tag{3.2a}$$

$$y = A \sinh(\nu) \sin(\Phi)/[\cosh(\nu) - \cos(u)], \tag{3.2b}$$

$$z = A \sin(u)/[\cosh(\nu) - \cos(u)]. \tag{3.2c}$$

The coordinates are restricted to the domain: $\nu \in [0,\infty]$, $u \in [0,2\pi]$, and $\Phi \in [0,2\pi]$. Here, if "a" denotes the mean radial distance to the toroid from the center, and "b" the thickness of the torus in the z = 0 plane, then the toroidal surface is given by values of constant $\nu = \nu_0 = \mathrm{Ln}[(a/b)+\{(a/b)^2-1\}^{1/2}]$, and also satisfies the equation: $z^2 + [(x^2 + y^2)^{1/2} - A \coth(\nu_0)]^2 = [A/\sinh(\nu_0)]^2$. In this notation, the parameter A of equation (3.2) is related to the mean radial distance "a" as: $A = a \tanh(\nu_0)$, and also to the parameter "b" as: $A = b \sinh(\nu_0)$. Thus, in this system, distances from the center (in the z=0 plane) to the inner and outer rims of the torus are "a-b" and "a+b", respectively. The inverse transformations are given by:

$$\Phi = \tan^{-1}(y/x), \tag{3.3a}$$

$$\nu = \mathrm{Ln}(d_1/d_2), \tag{3.3b}$$

$$u = \cos^{-1}[\{d_1^2 + d_2^2 - 4A^2\}/(2\, d_1 d_2)], \tag{3.3c}$$

where

$$d_{1,2} = [(x^2 + y^2)^{1/2} \pm A)^2 + z^2\,]^{1/2}. \tag{3.3d}$$

Here, the toroidal ring is taken to be charged and held at a constant potential V_0. The potential around the ring can then be conveniently obtained by solving the Laplace

equation, with the assumption that the deep-space environment has no atmosphere and negligible charge density. The governing equation can be written [59] as:

$$\{\delta[\sinh(v)\,\delta F/\delta v]/\delta v\}/\sinh(v) + \delta^2 F/\delta v^2 + \{\delta^2 F/\delta \Phi^2\}/\sinh^2(v) + F/4 = 0, \qquad (3.4)$$

where the required voltage $V(v,u,\Phi)$ is expressed in terms of $F(v,u,\Phi)$ as: $V = [\cosh(v)-\cos(u)]^{1/2} F(v,u,\Phi)$. The solution to this Dirichlet problem then works out to:

$$V(v,u,\Phi) = \left(\frac{V_0}{\pi}\right)[2\{\cosh(v)-\cos(u)\}]^{1/2}{}_{n=0}\sum^{\infty}[Q_{n-1/2}(\cosh(v_0))/P_{n1/2}(\cosh(v_0))]P_{n1/2}(\cosh(v))\cos(v), \quad (3.5a)$$

In the above, $P_{n-1/2}(x)$ and $Q_{n-1/2}(x)$ are the Legendre functions of the first and second kind, respectively, of degree "n-½".

Based on the solution from equation (3.5a), results for the potential due to a toroidal ring with mean radius a = 45 meters, thickness b = 10 meters, with its surface held at 300 MV are shown in Fig. 3-3. The surface voltage of 300 MV was taken to match the value reported in the literature [57]. As expected the values are the highest in the equatorial plane and fall off along with distance along either direction of the z-axis.

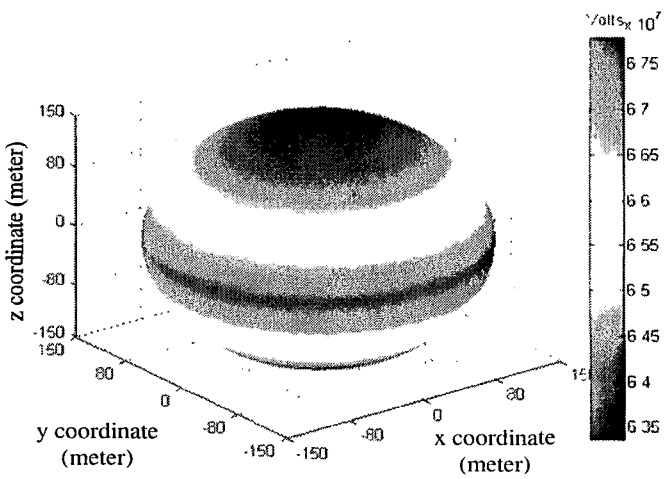

Fig. 3-3. Potential profile of a toroidal ring held at a 300 MV potential.

Based on equation (3.5a), the charge Q on each ring required to maintain the toroidal structure at a particular value of constant potential V_0 can be obtained through Gauss' law. Thus,

$$Q = \varepsilon_0 \iint E\, h_v\, h_\Phi\, d\Phi\, du, \tag{3.5b}$$

where h_u and h_Φ are the scale factors (or metric coefficients from which the Lame´ factors can be obtained) associated with the differentials "du" and "dΦ". For the toroidal system chosen:

$$h_u = h_v = A/[\cosh(v) - \cos(u)], \tag{3.5c}$$

$$\text{and} \quad h_\Phi = A \sinh(v)/[\cosh(v) - \cos(u)]. \tag{3.5d}$$

Here since dV/dv is independent of Φ, and hence one gets:

$$Q = -2\pi\varepsilon_0 A \int_0^{2\pi} \{(dV/dv)\, \{\sinh(v_0)/[\cosh(v_0) - \cos(u)]\}\, du \equiv Q(V_0). \tag{3.5e}$$

Since the potential around the ring is determined by the bias V_0 [as given in eqn. (3.5a)], the dV/dv term in eqn. (3.5e) implicitly involves this applied voltage [i.e., $Q \equiv Q(V_0)$]. Consequently, the total charge becomes a function of V_0. The electric field E normal to the constant $v = v_0$ surface, required in Eqn. (3.5b) can be obtained in a straight-forward manner as:

$$E = -(dV/dv)/h_v = -(dV/dv)\,[\cosh(v) - \cos(u)]/A. \tag{3.5f}$$

Thus by computing the total charge $Q(V_0)$ on the ring at a given voltage, the energy expended to build up the requisite potential [$= Q(V_0)\, V_0/2$] can easily be computed.

In these calculations, three toroidal rings were used with their axes of symmetry along the x-, y- and z-directions. The potential along the <111> direction for such a three-ring configuration (with all three surfaces held at 300 MV) is shown in Fig. 3-4. For comparison, the potential profile along this same <111> direction for a six-sphere configuration positioned on either sides of the three axes and held at 300 MV is also shown. To maintain some degree of geometric equivalence between the two configurations, each sphere was taken to have a radius of 10 meters with their centers on the three axes located 50 meters from the center. The profile of Fig. 3-4 brings out the advantage of the toroidal configuration. The potential is seen to be much higher with a sharper gradient (especially for the shorter distances) which create larger electric fields.

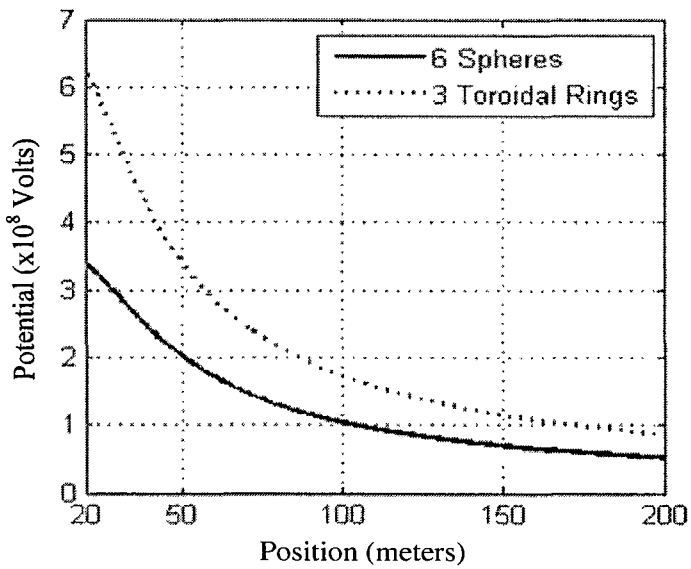

Fig. 3-4. Potential profile along the <111> direction for a three toroidal rings with each geometric surface maintained at a 300 MV bias. Potential for 6 spheres is also shown for comparison.

3.3 Forces and Equations of Motion due to Magnetostatic Fields

Perhaps a combination of the electrostatic and magnetostatic shielding might present a far superior alternative from the standpoint of radiation protection. A coupled, dual-approach could conceivable lower the field requirements due to mutual synergistic effects, and thus be a safer alternative. The lower field intensities would have the added advantage of reduced power requirements. Here one possibility might be to probe a hybrid configuration that uses twelve electrostatic spheres, in concert with a current-carrying superconducting ring for a superimposed magnetic field. The geometry is shown in Fig. 3.5, and consists of six outer spheres held at a negative potential ($-V_{neg}$), six inner spheres held at a positive potential (V_{pos}), and superconducting ring (carrying a loop current I) for providing the magnetic field. The innermost blue sphere denotes the volume to be shielded. The six outer negatively charged spheres are designed to play a role in repelling the free electrons from the solar wind [60].

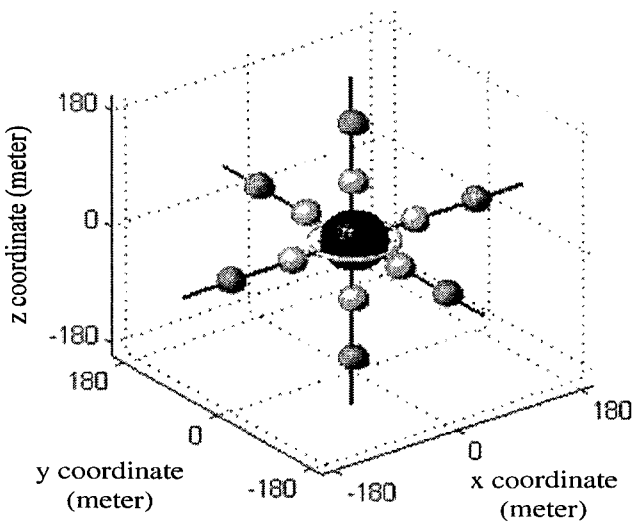

Fig. 3-5. Geometry considered for a dual electrostatic-magnetostatic shielding configuration.

Without such protection against the negative charge, three potential problems could arise: (a) electrons accelerated due to the positive potential would become dangerous to the astronauts and pose substantial health risks, (b) the acceleration would lead to excessive Bremsstrahlung levels, and (c) the electron current collected by the shielding elements (e.g., the toroidal rings) held at positive potential would annihilate the charge and lead to enhanced power requirements to maintain an effective electrostatic shield.

As regards a magnetic field, it has been shown [54] that a toroidal region exists around the center of a dipole magnetic field from which particles of a given energy are excluded. However, recent calculations have shown that the shielded region near the center of a current carrying loop is diminished as the radius of the coil increases [20]. Such analysis seems to suggest that deployed current carrying coils alone may not be very effective as magnetic shields, especially from high energy from GCR radiation. However, a combination of a magnetic current loop and charged electrostatic spheres (e.g., Fig. 3-5) might present a better design.

In this section then, we discuss the modifications to the equations of motion that will become necessary to include the presence of a magnetic field. Such a magnetic field will, for example, be produced by the current carrying rind shown in Fig. 3-5. The equation of motion for the incident charged particles due to a combination of electrostatic fields E and magnetic fields B having Cartesian components E_x, E_y, and E_z and B_x, B_y, and B_z, respectively, are given by:

$$\gamma\, m_x\, dv_x/dt = q\,[E_x + (v_y\, B_z - v_z\, B_y)\,], \tag{3.6a}$$

$$\gamma\, m_y\, dv_y/dt = q\,[E_y + (v_z\, B_x - v_x\, B_z)], \tag{3.6b}$$

and $\gamma\, m_z\, dv_z/dt = q\,[E_z + (v_x B_y - v_y B_x)]$. (3.6c)

The magnetic field components B_x, B_y, and B_z for a current carrying loop of radius "a" oriented in the x-y plane can easily be computed from the Biot-Savart law, yielding:

$$B_z = [\mu_0 I/(2\, a\, \pi\, Q)]\ [E(k)\ \{1 - \alpha_1^2 - \alpha_2^2\}/\{Q - 4\alpha_1\} + K(k)], \quad (3.7a)$$

$$B_x = \cos(\varphi)\ [\mu_0 I\, \alpha_3/(2\, a\, \pi\, Q)]\ [E(k)\ \{1 - \alpha_1^2 - \alpha_2^2\}/\{Q - 4\alpha_1\} + K(k)], \quad (3.7b)$$

and $$B_y = \sin(\varphi)\ [\mu_0 I\, \alpha_3/(2\, a\, \pi\, Q)]\ [E(k)\ \{1 - \alpha_1^2 - \alpha_2^2\}/\{Q - 4\alpha_1\} + K(k)], \quad (3.7c)$$

where I is the current in the superconducting loop, μ_0 is the free-space permeability, a is the loop radius, $Q = (1 + \alpha_1)^2 + \alpha_2^2$, $\alpha_1 = [(x^2 + y^2)^{1/2}]/a$, $\alpha_2 = z/a$, $\alpha_3 = z/[(x^2 + y^2)^{1/2}]$, $k = (4\alpha_1/Q)^{1/2}$, $\varphi = \tan^{-1}(y/x)$, while K(k) and E(k) are the complete elliptic integrals of the first and second kind, respectively. Here for computational simplicity, the elliptic integrals were evaluated using an approximation based on the three-point Gauss quadrature [61]:

$$K(k) = 0.512/(1 - 0.776\, k^2)^{1/2} + 0.258/(1 - 0.987\, k^2)^{1/2} + 0.8/(1 - 0.177\, k^2)^{1/2}, \quad (3.8a)$$

and $$E(k) = 0.232\ (1 - 0.993\, k^2)^{1/2} + 0.707\ (1 - 0.115\, k^2)^{1/2} + 0.632\ (1 - 0.751\, k^2)^{1/2}. \quad (3.8b)$$

3.4 Monte Carlo Simulations for Particle Trajectories

Calculations for charged particle penetration into the shielding structure to gauge its effectiveness can be performed based on Monte Carlo simulations for the specified configurations. These include either the toroidal or spherical geometries for the electrostatic cases, or the spherical and current-ring set up for the hybrid shielding case. The kinetic-based, Monte Carlo numerical simulations were used to follow the trajectories of 10,000 particles. These particles were taken to be injected inwards at random angles from a spherical simulation boundary of radius 150 meters. Trajectories

of each ionized particle were computed based on the relativistic equations of motion. The electrostatic driving force (= $-q \sum \nabla V_i$) from the three toroidal rings, as well as the spheres, was dynamic, based on the instantaneous position of the particle from the charged surfaces. By tracking the trajectories of all the 10,000 simulated particles, this process naturally allowed for the evaluation of the fraction penetrating the central region, those completely deflected by the electrostatic shielding arrangement, and the fraction incident onto the charged rings. The latter helps provide a measure of the rate of charge annihilation (and hence, voltage discharge) for a given space-environment and flux density for the spherical and toroidal geometries.

In order to accurately gauge space radiation responses to the shielding system via the Monte Carlo simulations, one has to first mimic the characteristics of both solar particle events (SPEs) and galactic cosmic rays (GCRs), and their respective energy-dependent fluxes. The solar activity cycle is approximately 11 years long [62] with about seven years of solar maximum. The published compilation of fluence spectra for the larger solar particle events [63] can serve as a convenient data set. It is believed that there are two categories of solar particle events and that each one accelerates particles in a distinct manner [64]. Solar flares have characteristics that tend to be electron rich, last for hours, and have unusually high ^{3}He content relative to ^{4}He and have low energy. On the other hand, Coronal Mass Ejection (CME) is a large eruption of plasma that drives a shockwave outward, tends to be proton rich, last for days, and has small ^{3}He content relative to ^{4}He and are of higher energy range of up to a hundreds of MeV range and are often used for testing radiation shield design. Here, for a more realistic and critical simulation assessments of the shielding capability for the electrostatic configurations, the

longer-term CME events were used. A description of the integral SPE flux φ used here can be expressed as Webber spectrum [65]:

$$\Phi = 10^9 \exp[\{239.1 - (E(E+1876))^{1/2}\}/100] \quad \#particles/cm^2 \quad (3.9)$$

For GCR, the model spectra of Badhwar and O'Neill [43] was used here since it is commonly used for space missions design investigations. A sample plot of the energy-dependent differential flux for galactic cosmic ray radiation is shown in Fig. 3.6 for a few representative ions. The peak is seen to occur at energies slightly below 1 GeV per nucleon.

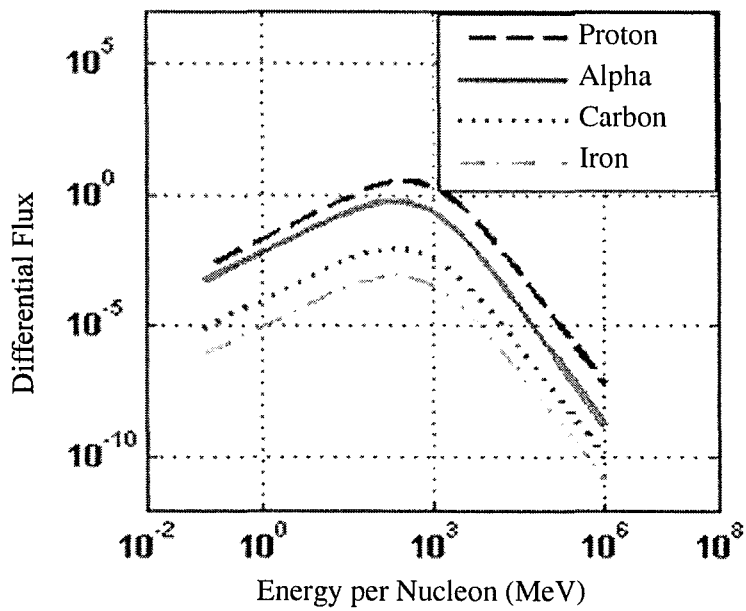

Fig. 3-6. Plot of the differential flux for a few select ions comprising the GCR spectra.

CHAPTER 4

RESULTS AND DISCUSSION

4.1 Introduction

In this chapter, the methodology described and discussed in the previous chapter will be used to simulate the penetration of incident charged space-particles through some select shielding systems. First, all-electrostatic systems will be analyzed with a couple of different geometries. Next, the results will be presented for a hybrid electrostatic-magnetostatic system. The simulation predictions will again be analyzed, and differences between the two approaches will be discussed.

4.2 Results and Analyses for the Electrostatic Shielding Systems

Numerical simulations were carried out to obtain particle trajectories based on equations given in the previous chapter. Each incident ion was taken to have the same initial starting energy, but assigned random position on a starting spherical surface. The initial velocities were also chosen to have random components, but in an inward direction. The Crank-Nicholson scheme was used which is an implicit, second-order method in time, and is numerically stable. A very small time step of 2 pico-seconds was chosen.

First, Monte Carlo based results for the 12-sphere configuration was obtained. For clarity, the 12-sphere configuration is shown again in Fig. 4-1(b), while Fig. 4-1(a) shows three toroidal rings in conjunction with six outer negatively charged spheres. The corresponding simulation results obtained for SPE and GCR protons for the 12-sphere configuration are given in Fig. 4-2.

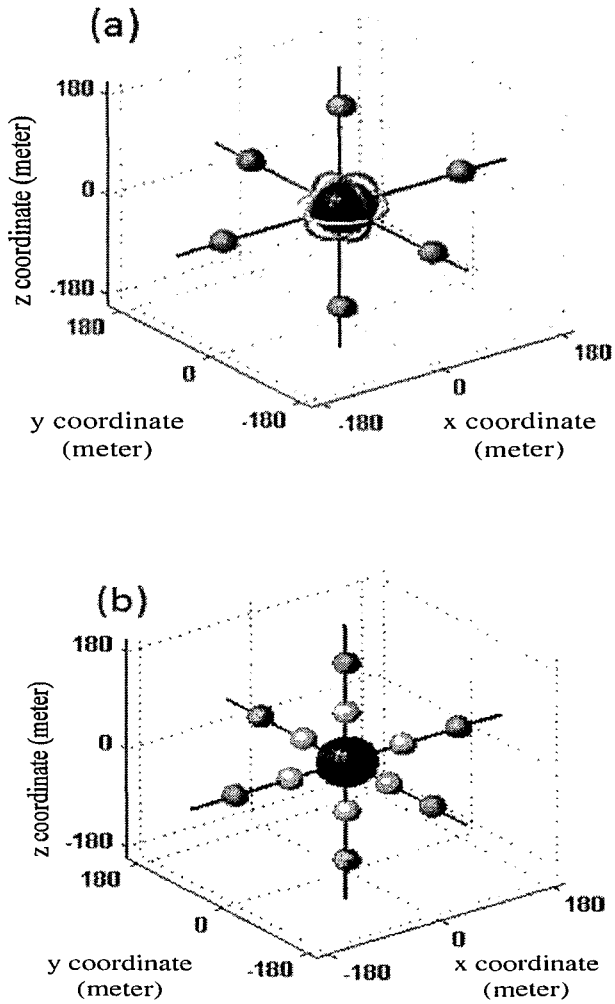

Fig. 4-1. Geometries considered for electrostatic shielding. The twelve-sphere configuration is shown in 4-1(b).

For concreteness the differential flux and the probability of protons hitting any one of the six outer negatively charged spheres are both shown. These calculations are important since one can gauge the amount of incident particles that would collide with and hit the spheres. Any such collision will lead to charge alteration, and hence, the possible annihilation of the charging potential on the spheres. From a practical standpoint, such

annihilation would need constant re-charging, and hence, the replenishment of energy from a suitable source.

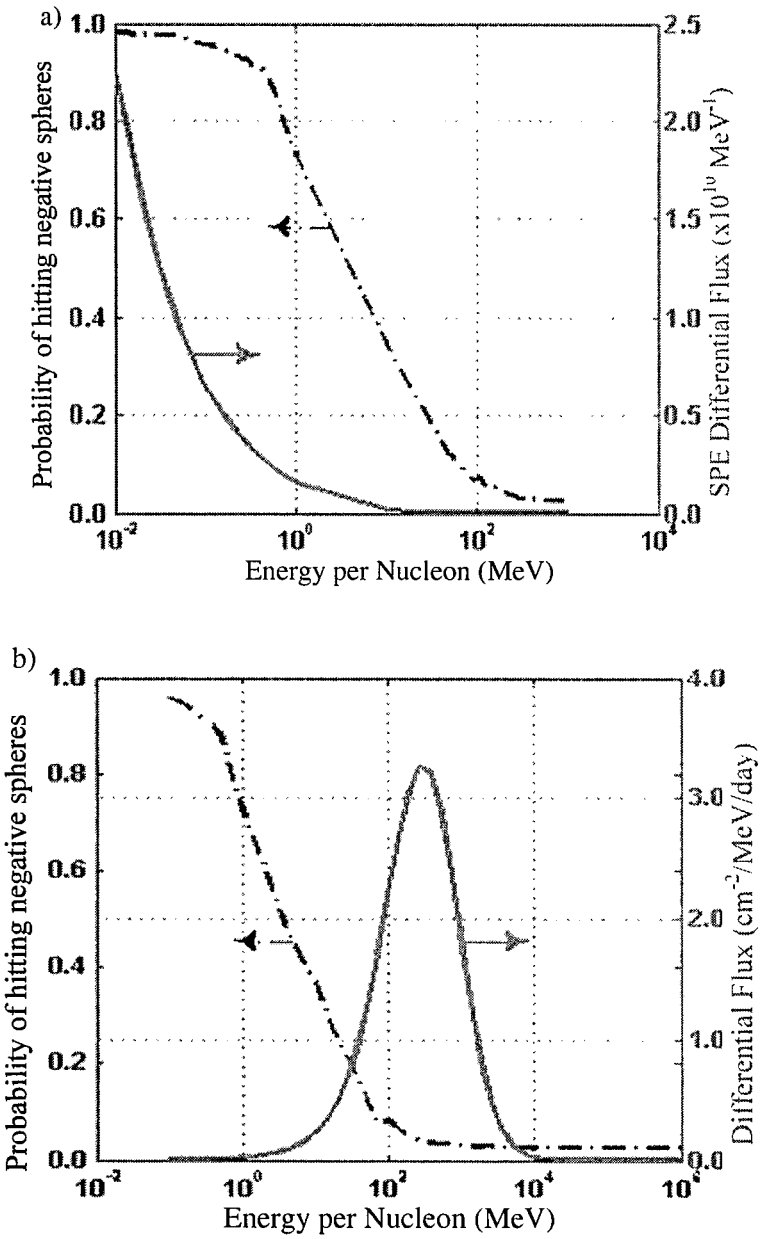

Fig. 4-2. Differential flux and computed probability of proton capture by the set of twelve charged spheres due to: (a) SPE radiation, and (b) protons from incident GCR flux.

The re-charging can thus amount to burdensome costs to the running of the overall system, and should be as minimal as possible. In the calculations, the six outer negatively charged spheres (as shown in Fig. 4-1b) were taken to be at a -100 MV potential, while the six inner positively charged spheres were each set at 100 MV. The radii of the outer and inner spheres were 20 and 10 meters, respectively, and their locations were at mean distances of 160 and 50 meters, respectively, from the center. As might be expected, at lower energies there is a stronger possibility for the protons to be captured by the set of six negatively charged outer spheres. These results can be used to evaluate the voltage discharge rate of the negative spheres and allows the average power loss from SPE collisions of various ions to be obtained.

Extending the calculations to alpha particles and iron ions in the GCR spectra yielded the results shown in Fig. 4-3. For GCR, the probability and flux curves have much less overlap (as compared to SPE), which is indicative of a negligible contribution to voltage discharging. The reduced overlap decreases the probability of a collision with the outer negative spheres, and makes voltage discharging (and hence the need to replenish and re-power the negative spheres) even more negligible. Overall, our calculations for SPE protons yielded a reduction of only ~1.163 Volts per Solar Particle Event based on the numerical values of the "hitting probability". This is clearly negligible compared to the assumed 100 MV initial bias. The computed values of power loss from GCR particle collisions were: 0.16462 mW (due to protons), 0.07234 mW (for alpha particles), and 1.587 μW (for Iron ions).

Next, predictions of the three-toroidal ring configuration [Fig. 4-1(a)] were compared to the results of the all-sphere geometry [Fig. 4-1(b)]. For a realistic head-to-

head comparison, the energy requirement for the two configurations was intentionally maintained at the same fixed level. This meant adjusting the equipotential across each of the three rings, and was carried out as follows.

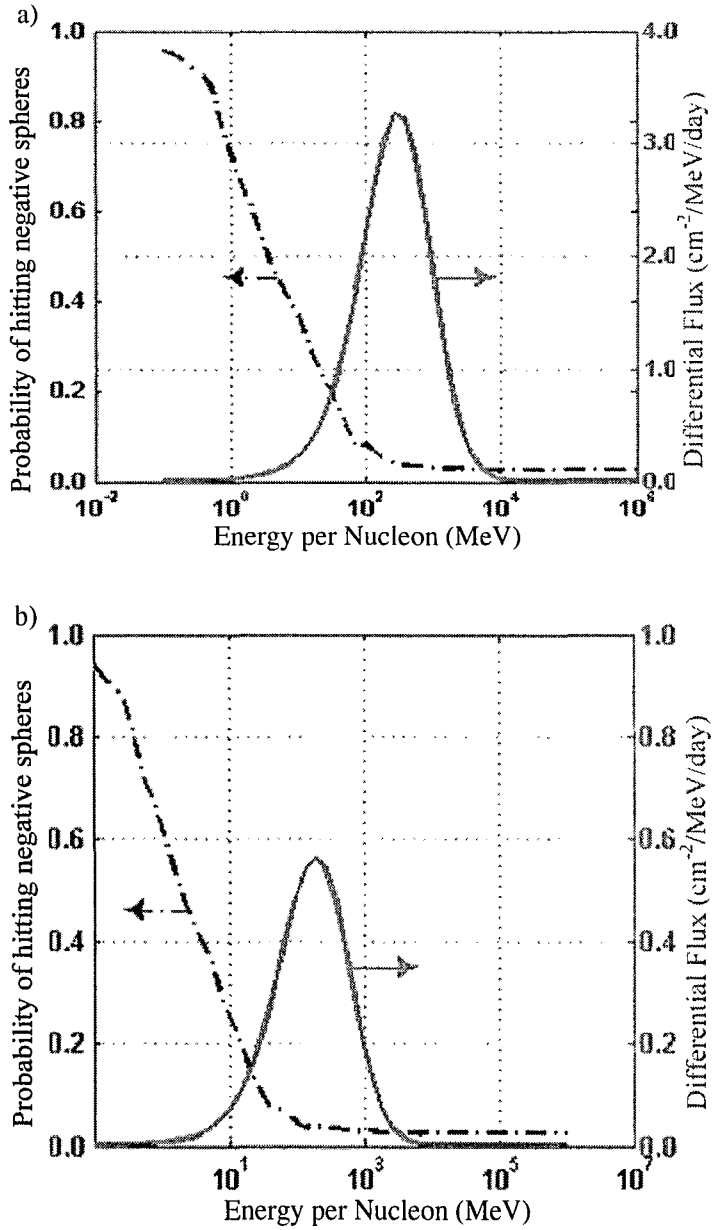

Fig. 4-3. Differential flux and computed probability of alpha and iron ion capture by the negatively charged spheres due to incident GCR flux. (a) Incident alpha particles, and (b) iron ions. The differential flux is also shown for clarity.

First, for the all-sphere configuration, the charge Q associated with a positive sphere of radius "a" (= 10 meters) held at a potential V_0 of +100 MV was computed as: $Q = 4\pi a\varepsilon_0 V_0 = 0.11121$ Coulombs. For the 6 inner positive spheres, this then leads to an overall energy of 3.3363×10^7 Joules [$= 6(0.5\ Q\ V_0)$]. An equivalent energy for the ring toroidal configuration, then places a condition on the potential V_0 such that: $0.5 \times V_0\ Q(V_0) \times 3 = 3.3363 \times 10^7$ as well in order to match the energy for the all-sphere configuration. Using equations 3.5(e) - 3.5(f) these quantities can be evaluated. The results upon numerical evaluation for the three toroids at "a" = 45 meters and "b"= 10 meters, yield a potential of about 50 MV for equivalent energy.

To gauge the performance based on this common energy requirement, simulations were carried out to compare proton transmission probabilities for the configuration involving the 6 negative and 6 positive spheres held at $\pm$ 100 MV, and the alternate geometry consisting of 3 rings at 50 MV and 6 outer negative spheres held at -100 MV. As mentioned above, the radii of the inner positive spheres were 10 meters, while the "a" and "b" parameters for the three toroids were taken to be 45 meters and 10 meters, respectively. As evident from Fig. 4-4, a significant lowering in the transmission probability is predicted for the configuration involving the three inner toroids. This reduction occurs at the high particle energies beyond the 200 MeV range, a regime that typically applies to GCR radiation. This reduction is occurs in spite of the toroidal voltage having been reduced down to +50 MV from the +100 MV value for the six-positive sphere case. Furthermore, though not explicitly shown here, further benefits can be expected by also replacing the six outer negative spheres by three corresponding negatively charged toroidal rings having a suitably larger radius "a".

Finally, for completeness, the role of structural dimensions for the toroidal rings was examined. One expects a torus with a larger radius to be better able to block incoming ions given its larger volume. In order to probe this quantitatively, simulations were performed for incoming protons for the three-ring configuration at the same 50 MV biasing, but for different values of the b-parameter for the toroidal ring. The results are shown in Fig. 4-5. With increasing value of the radial parameter b, the transmission probability is predicted to progressively decrease. In fact for a=45, the limiting probabilities drop from ~0.95 for b=1 meter down to ~0.45 at b=10 meters.

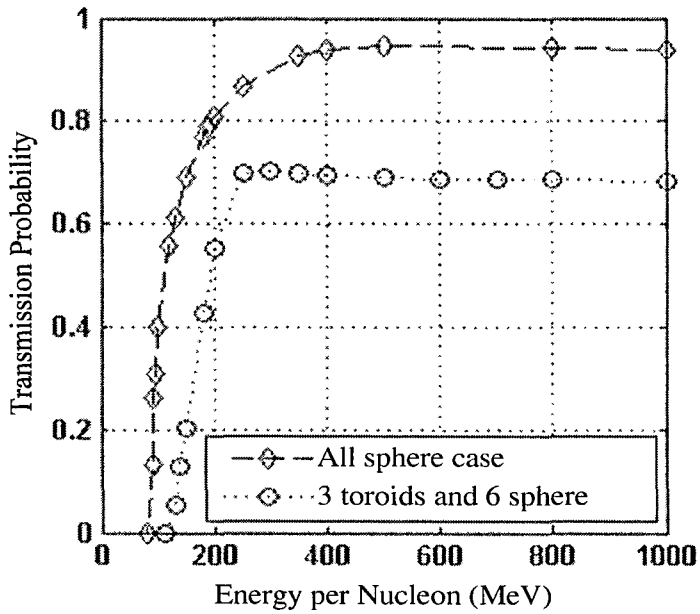

Fig. 4-4. Predicted transmission probabilities of GCR protons to penetration through an inner 20 meters spherical zone. Simulations were aimed at comparing the all sphere geometry of Fig. 4.1(b) and the toroidal configuration of Fig. 4.1(a) based on an equal-energy criteria.

This not only underscores the inherent advantage of the toroidal structure, but points towards construction of larger radii tori for more effective electrostatic active shielding.

The only conceivable downside might be in terms of the larger size and volume of the shielding structure. However, if advances in the flexible gossamer materials (or even mesh-like structures) are employed to advantage, this possible inconvenience associated with a larger structural mass can be overcome. It may be mentioned that the transmission probability in the 700-1000 MeV range over which the GCR spectra peaks is substantially reduced. For concreteness and clarity, the GCR spectra is shown below in Fig. 4-6.

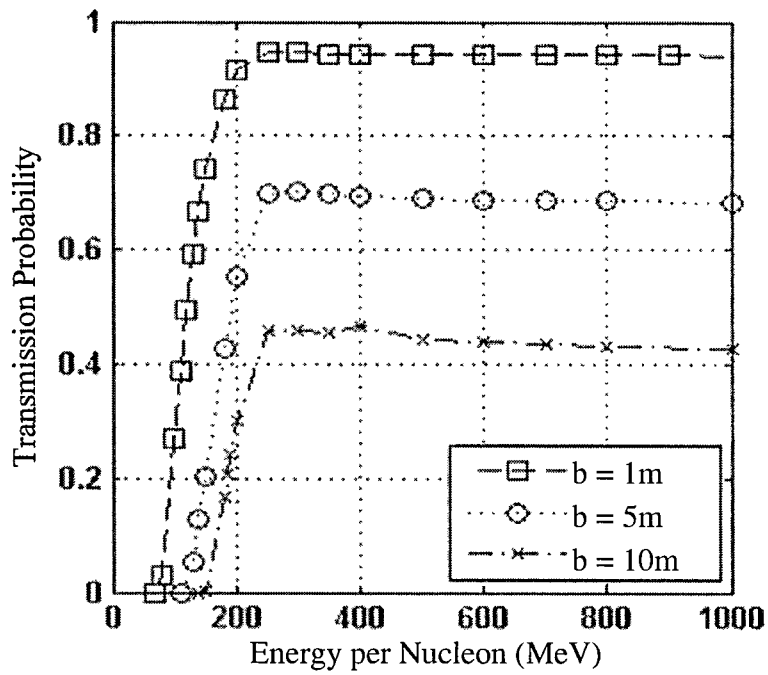

Fig. 4-5. Predicted proton transmission probabilities for the three-ring toroidal configuration for a = 45 meters, but for three different values of the b-parameter.

The y-axis shows the differential flux of the positive GCR particles, while the energy per nucleon is given on the x-axis. For different constituents of the GCR spectra, protons,

helium ions, carbon ions, and iron ions, representing the different ions present in the galactic cosmic ray distribution are shown in Fig. 4-6.

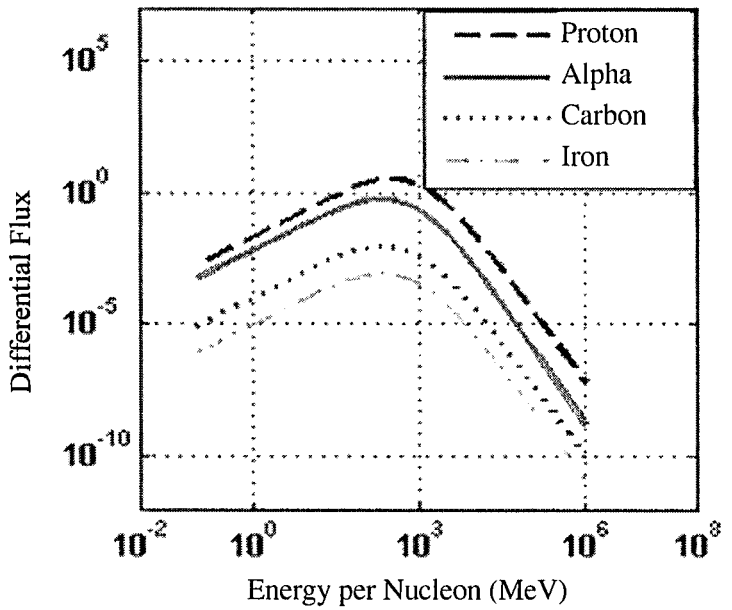

Fig. 4-6. Plot of the differential flux for a few select ions comprising the GCR spectra.

4.3 Results and Analyses for the Hybrid Shielding System

As already mentioned, perhaps a combination of the electrostatic and magnetostatic shielding might present a far superior alternative from the standpoint of radiation protection. A coupled, dual-approach could conceivable lower the field requirements due to mutual synergistic effects, and thus be a safer alternative. The lower field intensities would have the added advantage of reduced power requirements. Here one possibility might be to probe a hybrid configuration that uses twelve electrostatic spheres, in concert with a current-carrying superconducting ring for a superimposed magnetic field. The geometry is shown in Fig. 4.7, and consists of six outer spheres held

at a negative potential ($-V_{neg}$), six inner spheres held at a positive potential (V_{pos}), and superconducting ring (carrying a loop current I) for providing the magnetic field. The innermost blue sphere denotes the volume to be shielded. The six outer negatively charged spheres are designed to play a role in repelling the free electrons from the solar wind.

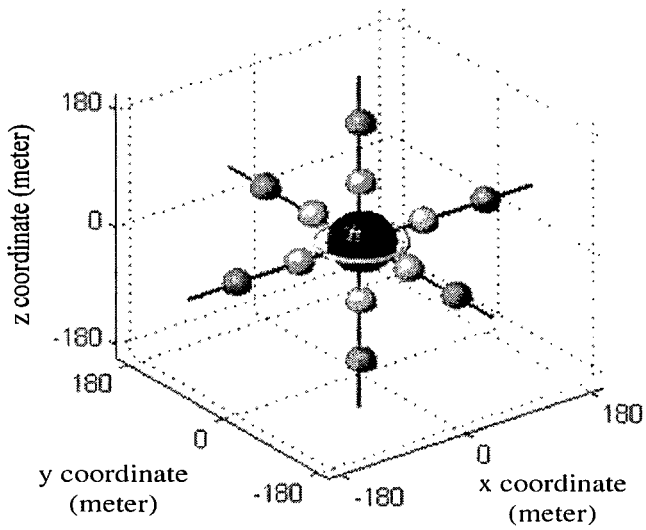

Fig. 4-7. Geometry considered for a dual electrostatic-magnetostatic shielding configuration.

Simulation results were obtained for the configuration of Fig. 4-7 that included twelve charged spheres and one current-carrying ring. The six outer negatively charged spheres were taken to be at a -100 MV potential, while the six inner positively charged spheres were each set at 100 MV. These voltages, incidentally, are much lower than the values of $\pm$ 300 MV chosen for the all-sphere, electrostatic scheme by Tripathi et al. The lower voltage values reduce the energy requirement, and so as such represent an improvement. The radii of the outer and inner spheres were 20 and 10 meters,

respectively, and their located at mean distances of 160 and 50 meters, respectively from the center. The inner zone to be protected was taken to be a spherical region of radius 20 meters. An important task in the design of the chosen hybrid shielding system is to determine the radius and current through the ring for optimal deflection of the incident ions. A larger current would produce a higher magnetic field, and be a more effective active shield. However, caution has to be exercised to ensure that the magnetic field values within the spherical shielded region produced by the ring are below the safety threshold of 0.5 Tesla [66]. The radius of the ring and the ring-current are also important design parameters. As will be shown in the numerical results, a larger ring radius helps keep the peak location of the magnetic field further away from the central protected zone. Under this situation, the current for a larger ring can then be increased to produce stronger magnetic fields further away, while still ensuring the peak value within the inner spherical protected zone (sphere of radius 20 meters), is below 0.5 Tesla. For the chosen configuration, though, the ring has a natural geometric constraint on the maximum radius due to the presence of the charged spheres. For the dimensions chosen, the radius can be at most 40 meters to avoid the ring from coming in contact with the a positive sphere.

Figure 4-8 shows the maximum values of the total magnetic field [$= (B_x^2 + B_y^2 + B_z^2)^{1/2}$] as a function of the ring current. These maximum magnetic field values were obtained both within the spherical protected zone of radius 20 meters, and for the overall simulated space. The ring radius for this calculation was set at 25 meters. The linear dependence is expected from equations (3.7(a) - 3.7(c)), but more importantly, the result shows that while a much higher magnetic field can exist (near the current-carrying ring for example), values within the inner protected zone as shown in Fig. 4-8 can be

significantly lower. This situation would serve the dual purpose of deflecting incident ions at distances far away from the center, while ensuring that the magnetic intensity within the inner 20 meters region remains within the 0.5 Tesla limit.

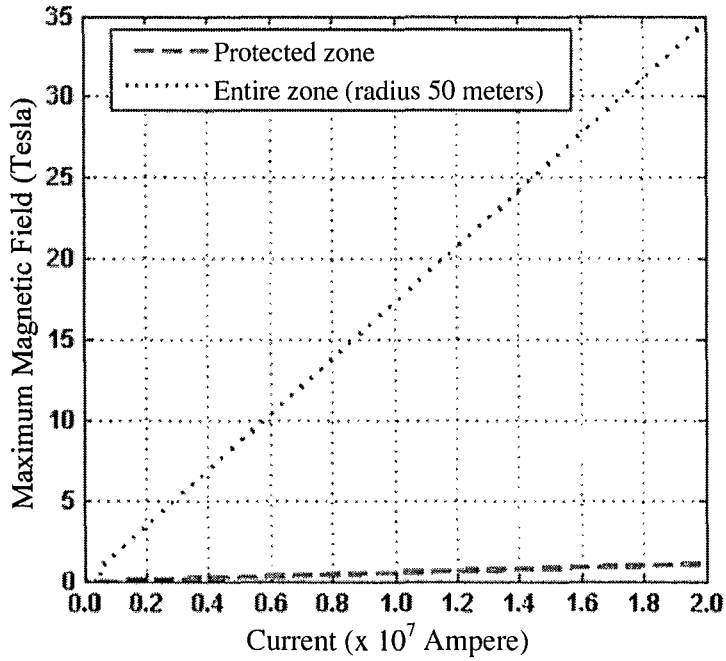

Fig. 4-8. Maximum magnetic field intensities due to a 25m ring as a function of its loop current. Values within a 50 meters region, and those within a 20m inner protected zone are shown.

Figure 4-9 shows the magnetic field distributions for two different ring radii of 25 meters and 40 meters, but with their currents adjusted so as to maintain the magnetic field at a maximum of value of 0.5 Tesla inside the 20 meters protected zone. The 25 meters radial ring had a current of 8.81×10^6 Amperes and produced the distribution of Fig. 4-9(a) with a maximum magnetic field of 15.27 Tesla. Besides the radial distance, only the polar angle has been shown in Fig. 4-9(a) due to the azimuthal symmetry. As apparent

from Fig. 4-9, the peak intensity occurs at the ring circumference and is in the plane of the ring (= angle of $\pi/2$) for both the ring radii.

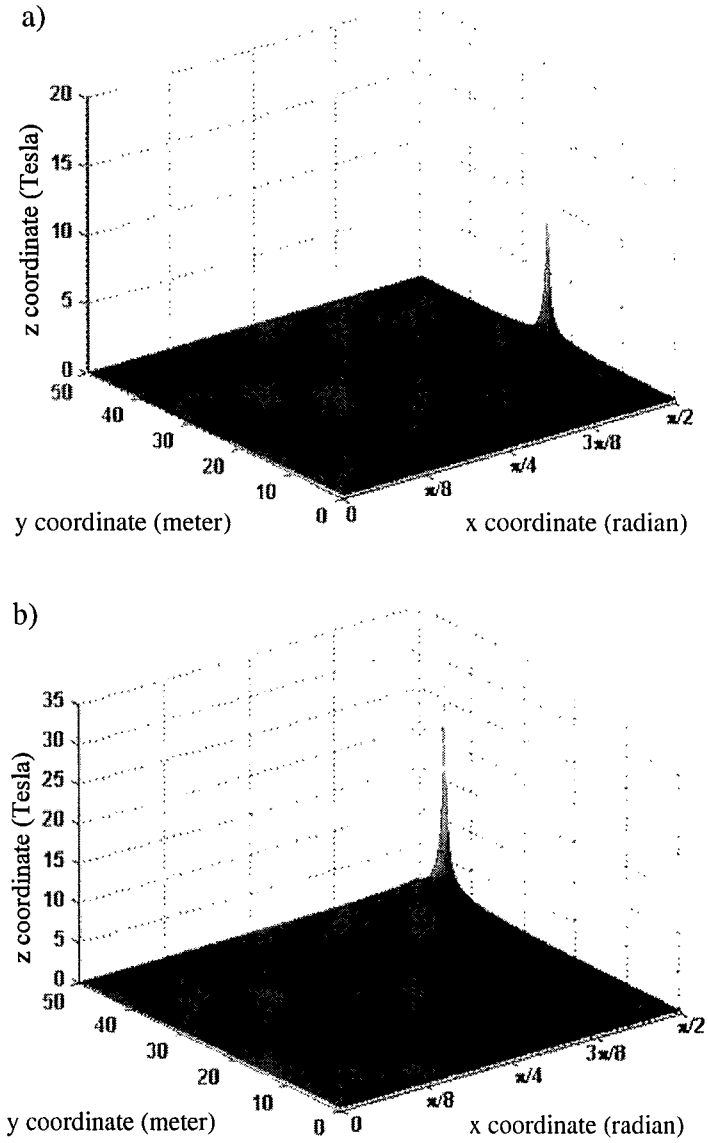

Fig. 4-9. Magnetic field intensity as a function of radial distance from the center and the polar angle for two different current-carrying rings. (a) 25m radius ring, and (b) a 40m radius ring.

For a 45 meters radius ring, the results of which are shown in Fig. 4-9(b), the peak value is predicted to be 34.25 Tesla. The maximum current for this ring size was taken to be 2.55×10^7 Amperes to ensure the magnetic intensity remained below the 0.5 Tesla limit within the protected zone. Thus for a larger ring radius, the magnetic intensity is much higher, though it still occurs in the plane of the ring at the circumference.

Numerical simulations were carried out for the 40 meters ring (in addition to the 12-spheres) based on equations (2) to obtain the trajectories of a collection of incoming ionized particles. Each incident ion was taken to have the same initial starting energy, but assigned random position on a spherical surface at a distance of 500 meters from the center. The starting velocities were all chosen to have random components, but in an inward direction. The Crank- Nicholson scheme was used which is an implicit, second-order method in time, and is numerically stable. A very small time step of 2 pico-seconds (psec) was implemented. Figure 4.10 shows the computed trajectories of 50 sample particles starting from random locations at the simulation surface 500 meters from the origin. Potentials of ± 100 MV were assumed for the positive and negative spheres, with a 2.55×10^7 Ampere circulating current in the ring set at a 40 meters radius. Each injected particle was assigned a 1000 MeV energy. The trajectories of Fig. 4-10 clearly reveal that most of the incident particles are successfully turned away from the central zone.

Next, results were obtained for the probabilities of incoming protons to enter the inner 20 meters radius region as a function of various incident energies. The simulated transmission probability into the inner zone is shown in Fig. 4-11. As done previously, the six outer and six inner spheres were set at a biasing of -100 MV and +100 MV, respectively, while the 40 meters ring was taken to have a 2.55×10^7 Ampere circulating

current. For a clearer comparison, Fig. 4-11(a) shows the transmission probability of protons for this configuration, with and without the current-carrying ring.

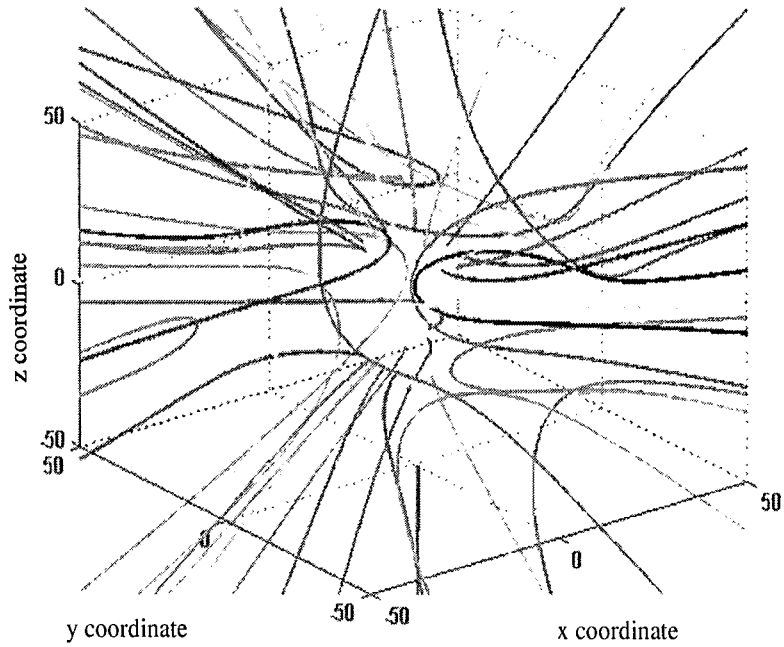

Fig. 4-10. Simulation result shows the representative 2000 MeV proton trajectories for the 1-ring and 12-sphere shielding configuration of Fig. 1-1.

The benefits of the hybrid system are obvious. Though the degree of deflection (and hence, transmitted fraction) is energy dependent, the hybrid system is better able to provide active at all energies. For example, 2000 MeV protons are predicted to have a penetration probability of almost ninety percent with electrostatic shielding alone, but a probability below sixty percent for the hybrid system. For completeness, the transmission probabilities of the hybrid electrostatic-magnetostatic system for a few other ions are also shown in Fig. 4-11(b). There were significant improvements over the simple electrostatic configuration in all cases. Most importantly, the transmission

probability is seen to be substantially reduced in the 700-1000 MeV range, a span where the GCR flux has its peak.

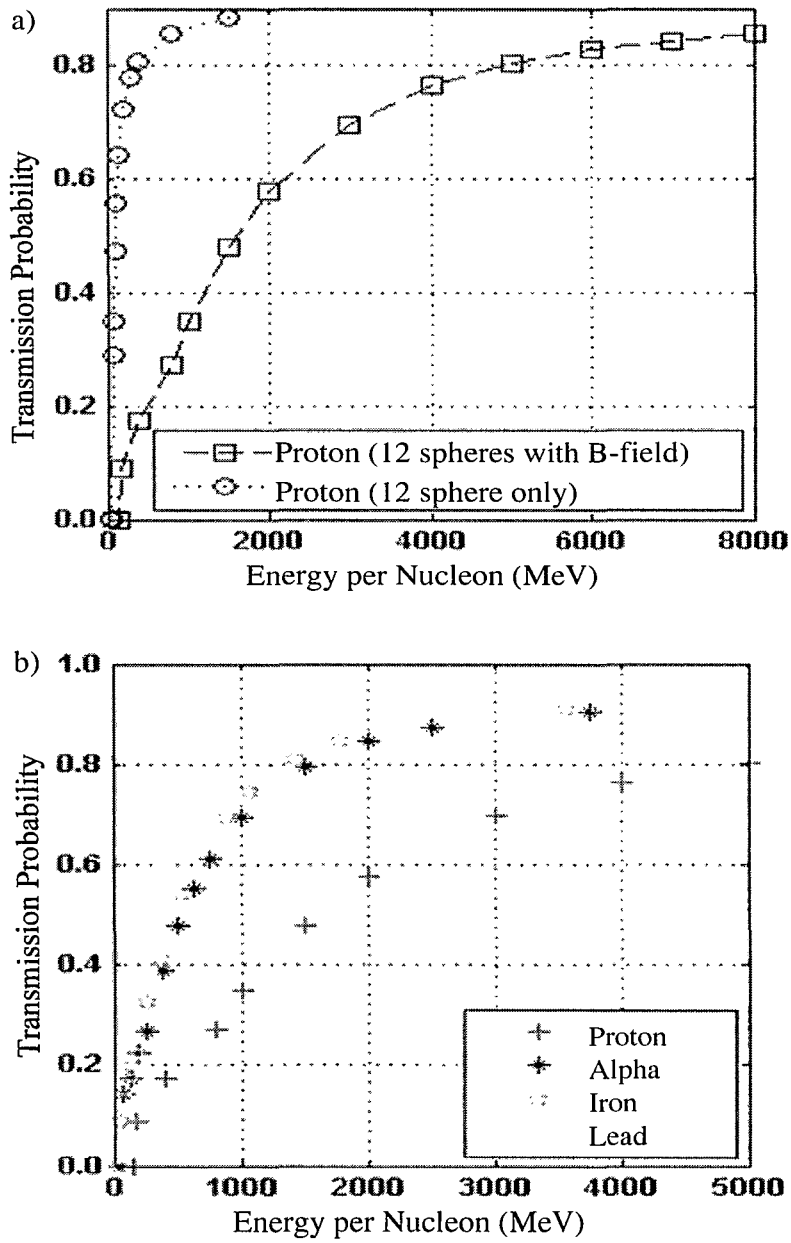

Fig. 4-11. Energy dependent probability of protons to penetrate through a 20 meters spherical zone for the 1-ring and 12-sphere shielding configuration. (a) Results for protons with and without the current-carrying ring, and (b) Transmission probability for the hybrid system for several ions.

The differential flux and the probability for protons to hit one of the six outer negatively charged spheres were also evaluated. This is an important calculation since it directly yields the amount of charge neutralization (and hence the voltage discharge) for the electrostatic component of the shielding system. These results, with and without the current-carrying ring, are shown in Fig. 4-12. They reveal, as might be expected, that at lower energies there is a stronger possibility for the protons to be captured by the set of six negatively charged outer spheres. However, differences between the all-electrostatic and hybrid systems exist with the hybrid system predict to have a lower probability of hitting the six negative spheres. So once again, from the standpoint of having to re-charge the electrostatic spheres, the hybrid configuration shows superior performance. Knowing the energy-dependent "hitting probabilities" allows the evaluation of the power loss from SPE collisions due to various incoming ion species.

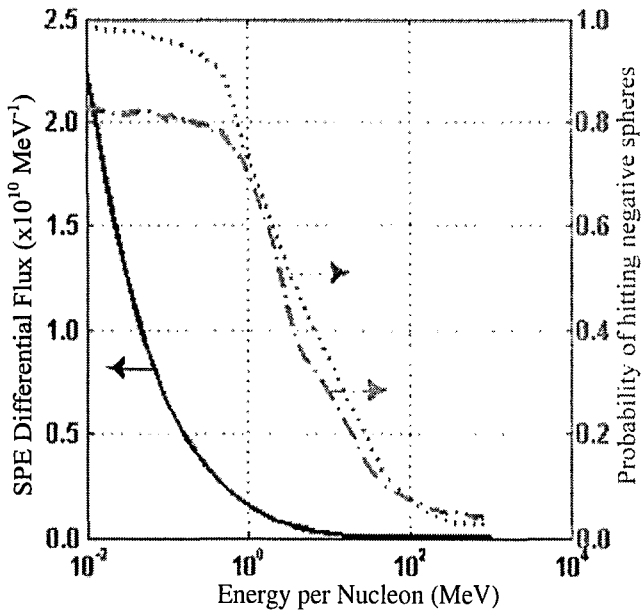

Fig. 4-12. Differential flux and computed probability of SPE proton capture for the hybrid (lower dashed curve) and 12-sphere all electrostatic (dotted curve) configurations.

Our calculations for SPE protons yielded a reduction of only 0.168 Volts. This is totally negligible as compared to the applied -100 MV potential. Hence, this shielding configuration is practically immune to any re-charging requirement from a solar particle event. This low discharge value is easily understood from the negligible overlap between the "hitting probability" and SPE differential flux curves. Repeating the above calculation for protons from the GCR characteristics yielded the plots shown in Fig. 4-13 that compare the hybrid and all-electrostatic systems. The computed value of power loss from GCR proton collisions was about 1.5 nano Watt (nW) and hence, totally negligible.

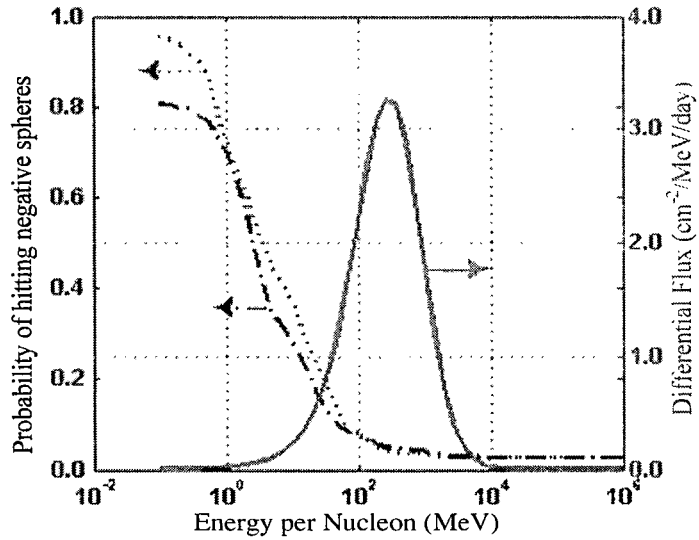

Fig. 4-13. Differential flux and computed probability of proton capture for the hybrid (dashed) and 12-sphere all electrostatic (dotted curve) configurations from incident GCR flux.

4.4 Summarizing Conclusions

Detailed simulation studies to evaluate a toroidal configuration for its potential towards electrostatic shielding were performed. A simpler all-sphere structure was

included to provide a reference and convenient comparison. The SPE radiation was shown to be almost eliminated by these electrostatic configurations. Furthermore, it was shown that the power needed to replenish the electrostatic charges on the all-sphere shielding configuration due to particle hits from the GCR and SPE radiation is minimal and insignificant. Most importantly, it was shown that novel structures such as toroidal rings appear to be very promising. Comparisons were also made between the two configurations at a fixed common energy. The results showed substantial improvements in shielding, even at the high energies above 200 MeV per nucleon.

Our study represents a simple first-step evaluation. Improvements are certainly possible by choosing other novel structures or meshed designs to reduce weight and costs while still achieving the requisite active shielding. More interestingly, the dimensions and aspect ratio of the spheres and/or toroidal rings could be altered to achieve an even higher degree of radiation protection. Finally, a simple extension can then be the replacement of the six outer negative spheres with three larger toroidal rings held at a negative potential.

In addition, numerical studies were also performed to evaluate the potential for a hybrid system for active shielding against space radiation. Most previous approaches have been based on a single concept alone, such as the magnetic, electrostatic or plasma shielding. However, all of the conventional approaches (including passive shielding) have potential problems. The main advantages seen for the hybrid system were: (i) much lower magnetic fields that could be below the thresholds set for health and safety for long-term exposures, and (ii) a much better shielding and repulsion of incident ions from

both SPE and GCR, and (iii) reductions in the power requirement for re-charging the electrostatic sub-system.

CHAPTER 5

CONCLUSION AND SCOPE FOR FUTURE WORK

5.1 Introduction

This final chapter summarizes the main aspects and elements of this thesis research. The contributions and novel features are highlighted. This work is merely represents the beginning of a more thorough and in-depth research into shielding for deep-space applications. The importance of such simulations is that a number of important aspect and alternative designs can quickly be evaluated and analyzed without having to build a costly system. In time, as an optimal design gradually emerges, actual testing of a possible prototype can be carried out. This chapter ends with a brief description of possible tasks for the future and scope for follow-up research work.

5.2 Summary of Thesis Work and Accomplishments

The health threat from cosmic rays is the danger posed by galactic cosmic rays (GCRs) and solar energetic particles to astronauts on interplanetary missions. Galactic cosmic rays consist of high energy protons (85%), helium (14%) and other high energy nuclei. Solar energetic particles consist primarily of protons accelerated by the sun to high energies via proximity to solar flares and coronal mass ejection. They are one of the most important barriers standing in the way of plans for interplanetary travel by spacecraft with crew.

Life on the Earth's surface is protected from galactic cosmic rays by a number of factors as given below:

1. The Earth's atmosphere is opaque to primary cosmic rays with energies below about 1 GeV, so only secondary radiation can reach the surface. The secondary radiation is also attenuated by absorption in the atmosphere, as well as by radioactive decay in flight of some particles, such as moons. Particles entering from a direction close to the horizon are especially attenuated. The world's population receives an average of 0.4 milli-Sieverts (mSv) of cosmic radiation annually (separate from other sources of radiation exposure like inhaled radon) due to atmospheric shielding. At 15 km altitude, above most of the atmosphere's protection, radiation dose as an annual rate rises to 20 milli-Sieverts (mSv) at the equator to 50 - 120 milli-Sieverts (mSv) at the poles, varying between solar maximum and minimum conditions.
2. Except for the very highest energy galactic cosmic rays, the radius of gyration in the earth's magnetic field is small enough to ensure that they are deflected away from Earth. Missions beyond low earth orbit leave the protection of the geomagnetic field, and transit the Vann Allen radiation belts. Thus they may need to be shielded against exposure to cosmic rays, Van Allen radiation, or solar flares. The region between two to four earth radii lies between the two radiation belts and is sometimes referred to as the "safe zone".
3. The interplanetary magnetic field, embedded in the solar wind, also deflects cosmic rays.

As a result the energy input of GCRs to the atmosphere is negligible — about 10^{-9} of solar radiation which is roughly the same as starlight.

In this thesis, detailed simulation studies to evaluate a toroidal configuration for its potential towards electrostatic shielding were performed. A simpler all-sphere structure was included to provide a reference and convenient comparison. The SPE radiation was shown to be almost eliminated by these electrostatic configurations. Furthermore, it was shown that the power needed to replenish the electrostatic charges on the all-sphere shielding configuration due to particle hits from the GCR and SPE radiation is minimal and insignificant. Most importantly, it was shown that novel structures such as toroidal rings appear to be very promising. Comparisons were also made between the two configurations at a fixed common energy. The results showed substantial improvements in shielding, even at the high energies above 200 MeV per nucleon.

Our study represents a simple first-step evaluation. Improvements are certainly possible by choosing other novel structures or meshed designs to reduce weight and costs while still achieving the requisite active shielding. More interestingly, the dimensions and aspect ratio of the spheres and/or toroidal rings could be altered to achieve an even higher degree of radiation protection. Finally, a simple extension can then be the replacement of the six outer negative spheres with three larger toroidal rings held at a negative potential.

In addition, numerical studies were also performed to evaluate the potential for a hybrid system for active shielding against space radiation. Most previous approaches have been based on a single concept alone, such as the magnetic, electrostatic or plasma shielding. However, all of the conventional approaches (including passive shielding) have potential problems. The main advantages seen for the hybrid system were: (i) much

lower magnetic fields that could be below the thresholds set for health and safety for long-term exposures, and (ii) a much better shielding and repulsion of incident ions from both SPE and GCR, and (iii) reductions in the power requirement for re-charging the electrostatic sub-system.

In addition to a numerical study of an all-electrostatic system, this thesis research also extended the shielding strategy to study a hybrid configuration based on both electrostatic and magnetostatic fields. The main advantages of this dual-system were shown to be: (i) a much better shielding and repulsion of incident ions from both solar particle events (SPE) and galactic cosmic rays (GCR), (ii) reduction in the power requirement for re-charging the electrostatic sub-system, and (iii) low requirements of the magnetic fields that are well below the thresholds set for health and safety for long-term exposure. Furthermore, the present results show transmission levels reduced to levels as low as 30% for energies around 1000 MeV, and near total elimination of SPE radiation by these hybrid configurations. It was also shown that the power needed to replenish the electrostatic charges due to particle hits from the GCR and SPE radiation is minimal. For example, the computed value of power loss from GCR proton collisions was about 1.5 nW and hence, totally negligible. The power loss from SPE collisions due to various incoming ion species was calculated, and for SPE protons, yielded a reduction of only 0.168 Volts. This is totally negligible compared to the 100 MV potential on the electrostatic system.

5.3 Scope for Future Work

Some basic and useful work through simulation analyses was carried out in the area of active shielding for deep-space applications. However, this represents only a

small start, and a number of issues still remain to be probed. As part of continuing effort in this area, the following tasks can be carried out in the future. These efforts would broaden the scope and improve the shielding protection from radiation for the astronauts.

1. Carry out systematic studies of varying the size of the toroidal rings with regards to both their mean radius, as well as changes in the applied potential. On the one hand, increasing the potential would repel more ions, but would come at the cost of enhanced energy and power requirements. So an optimal solution would be desirable.
2. Evaluate the trajectories and stopping power of mesh-like tori. Such mesh-like structure would save material and be lightweight for easier manipulation in space.
3. Determine the range of values of both the negative and positive potentials for the all-electrostatic system. It is very likely that changing the potential of one (say the positive voltage) would need subsequent modifications in the negative potential to achieve the desired level of protection. The changes in the potential need to be such that the greatest protection with the least energy loss due to particle strikes is achieved.
4. Conduct detailed studies of the dual hybrid system. This would mean changing the size and location of the electrostatic spheres, while altering the magnetic fields for maximum protection.
5. Use toroidal structures instead of spheres for the hybrid scheme, and evaluating the resulting performance predictions.
6. Look at other aspects such as the structural stability and practical requirements for any tethers for holding the shielding configurations in place.

REFERENCES

[1] Dudkin, V.E., Kovalev, E.E., Kolomensky, V., Sakovich, V.A., Semenov, V.F., Damis, V.P., Benton, E.V., Radiation Shielding Estimates for Manned Mars Space Flight. Nuclear Tracks Radiation Measurements, 20, pp. 29-32, 1992.

[2] Hoffman, S.J., Kaplan, D.I., Human Exploration of Mars: The Reference Mission of the NASA Mars Exploration Study Team. NASA Johnson Space Center, Houston, TX; NASA Special Publication 6107, 1997.

[3] Wilson, J.W., Cucinotta, F.A., Kim, M.H., Schimmerling, W., Optimized Shielding for Space Radiation Protection. Phys. Med. XVII (Suppl. 1), 2001.

[4] Vogler, F.H., Analysis of an electrostatic shield for space vehicles. AIAA Journal, 2, pp. 872–878, 1964.

[5] Levy, R.H., James, G.S., Plasma radiation shielding for deep space vehicles. Space Aeronaut, 45, pp. 106–120, 1966.

[6] Bernert, R.E., Stekly, F.J.J., Magnetic radiation shielding using superconducting coils, in: Second Symposium on Protection against Radiation in Space. NASA SP-71, pp. 199–209, 1965.

[7] Levine, S.H., Lepper, R., An active radiation shield for cylindrical shaped vehicles. Journal of Spacecraft and Rockets, 8, pp. 773–777, 1971.

[8] Townsend, L.W., HZE particle shielding using confined magnetic fields. Journal of Spacecraft and Rockets, 20, pp. 629–630, 1983.

[9] Sussingham, J.C., Watkins, S.A., Cocks, F.H., Forty years of development of active systems for radiation protection of spacecraft. Journal Astronaut Science, 47, pp. 165–175, 1999.

[10] Townsend, L.W., Overview of active methods for shielding spacecraft from energetic space radiation. Phys. Med. XVII-Suppl. 1, pp. 84–85, 2001.

[11] Cocks, F. H. A Deployable High Temperature Superconducting Coil (DHTSC): A Novel Concept for Producing Magnetic Shields Against Both Solar Flare and Galactic Radiation During Manned Interplanetary Missions. Journal British Interplanetary Soc., 44, pp. 99–102, 1991.

[12] Spillantini, P., Casolino, M., Durante, M., Mueller-Mellin, R., Reitz, G., Rossi, L., Shurshakov, V., Sorbi, M., Shielding from cosmic radiation for interplanetary missions: Active and passive methods. Radiation Measurements, 42, pp. 14 - 23, 2007.

[13] Kinouchi, Y., Yamaguchi, H., Tenforde, T.S., Theoretical analysis of magnetic field interactions with aortic blood flow. Bioelectromagnetics, 17, pp. 21-32, 1996.

[14] Kawakubo, T., Yamauchi, K., Kobayashi, T., Effects of magnetic field on metabolic action in the peripheral tissue. Journal of Applied Physics, Part 2: Letters, 38, pp. L1201-L1203, 1999.

[15] Nittby, H., Grafström, G., Eberhardt, J.L., Malmgren, L., Brun, A., Persson, B.R.R., Salford, L.G., Radiofrequency and extremely low-frequency electromagnetic field effects on the blood-brain barrier. Electromagnetic Biology and Medicine, 27, pp. 103-126, 2008.

[16] Kanokov, Z., Schmelzer, J.W.P., Nasirov, A.K., New mechanism of solution of the k_BT-problem in magnetobiology. Central European Journal Phys., 8, pp. 667-671, 2010.

[17] Salford, L.G., Nittby, H., Brun, A., Grafstrom, G., Malmgren, L., Sommarin, M., Eberhardt, J., Widegren, B., Persson, B.R.R., The mammalian brain in the electromagnetic fields designed by man with special reference to blood-brain barrier function, neuronal damage and possible physical mechanisms. Progress of Theoretical Physics Supplement, 173, pp. 283-309, 2008.

[18] Tripathi, R.K., Wilson, J.W., Cucinotta, F.A., Nealy, J. E., Clowdsley, M.S., Kim, M.Y., Deep space mission radiation shielding optimization. International Conference on Environmental Systems, Orlando, FL; SAE 01ICES 2326, 2001.

[19] ICNIRP, Guidelines for Limiting Exposure to Time-Varying Electric, Magnetic, and Electromagnetic Fields (Up to 300 GHz). Health Physics, 74, pp. 494-522, 1998.

[20] Shepherd, S.G., Kress, B.T., Stormer theory applied to magnetic spacecraft shielding. Space Weather, 5, S04001, 2007.

[21] Shepherd, S.G., Shepherd, J.P.G., Toroidal magnetic spacecraft shield used to deflect energetic charged particles. Journal of Spacecraft and Rockets, 46, pp. 177-184, 2009.

[22] Cucinotta, F.A., Manuel, F., Jones, J., Izsard, G., Murray, J., Djojonegoro, B., Wear, M., Space radiation and cataracts in astronauts. Radiation Research, 156, pp. 460–466, 2001.

[23] Preston, D.L., Shimizu, Y., Pierce, D.A., Suyumac, A., Mabuchi, K., Studies of mortality of atomic bomb survivors. Report 13: Solid Cancer and Noncancer Disease Mortality: 1950–1997. Radiation Research, 160, pp. 381–407, 2003.

[24] Howe, G.R., Zablotska, L.B., Fix, J.J., Egel, J., Buchanan, J., Analysis of the mortality experience amongst U.S. nuclear power industry workers after chronic low-dose exposure to ionizing radiation. Radiation Research, 162, pp. 517–526, 2004.

[25] NCRP, Recommendations of dose limits for low Earth orbit. NCRP Report 132, Bethesda, MD, 2000.

[26] NAS Space Science Board, Report of the Task Group on the Biological Effects of Space Radiation. Radiation Hazards to Crews on Interplanetary Mission National Academy of Sciences, Washington, DC, 1996.

[27] Reames, D.V., Particle acceleration at the sun and in the heliosphere. Space Science Reviews 90, pp. 417–491, 1999.

[28] Shea, M.A., Smart, D.F., History of energetic solar protons for the past three solar cycles including cycle 22 update, In: Biological Effect of Solar and Galactic Cosmis Radiation, Part B, Eds.: Swenberg, C.E., Horneck, G., Stassinopoulos, E.G. Plenum Press, pp. 37–71, New York, 1993.

[29] Nymmik, R.A., Radiation environment induced by cosmic ray particle fluxes in International Space Station orbit according to recent solar and galactic cosmic ray models. Advances in Space Research, 21, pp. 1689–1698, 1998.

[30] Nymmik, R.A., Probabilistic model for fluences and peak fluxes of solar particles. Radiation Measurements, 30, 287–296, 1999.

[31] Xapsos, M.A., Summers, G.P., Shapiro, P., Burke, E.A., New techniques for predicting solar proton fluences for radiation effects applications. IEEE Transactions on Nuclear Science, 43, pp. 2948–2953, 1996.

[32] Feynman, J., Spitale, G., Wang, J., Interplanetary proton fluence model: JPL 1991. Journal Geophys. Res. 98(A8), pp. 13281–13294, 1993.

[33] King, J.H., Solar Proton Fluences for 1977-1983 Space Missions. Journal Spacecraft, 11, pp. 401-408, 1974.

[34] Edwin, L.C., Shimizu, K., Lognormal distribution: theory and application. Statistics, textbooks and monographs, 88, 1988.

[35] Gabriel, S.B., Feynman, J., Power-law Distribution for Solar Energetic Proton Events. Solar Physics, 165, pp. 337-346, 1996.

[36] Shea, M.A., Smart, D.F., A Summary of Major Solar Proton Events. Solar Physics, 127, pp. 297-320. 1990.

[37] SIS ACE data. Retrieved from http://www.srl.caltech.edu/ACE/

[38] Simpson, J.A., Elemental and isotopic composition of the galactic cosmic rays. Annual Review of Nuclear and Particle Sciences, 33, pp. 323–382, 1983.

[39] Hörandel, J.R., The origin of galactic cosmic rays. Nuclear Inst. Methods in Physics Research, 588, Section A, pp. 181–188, 2008.

[40] Mrigakshi, A.I., Matthiä, D., Berger, T., Reitz, G., Wimmer-Schweingruber, R.F., Assessment of galactic cosmic ray models. Journal of Geophysics Research, 117, A08109, 2012.

[41] Katz, K., Ackerson, B., Homayoonfar, M., Sharma, S.C., Inactivation of cells by heavy ion bombardment. Radiation Research, 47, pp. 402–425, 1971.

[42] Tylka, A.J., Adams, J.J.H., Boberg, P.R., Brownstein, B., Dietrich, W.F., Flueckiger, E.O., Petersen, E.L., Shea, M.A., Smart, D.F., Smith, E.C., CREME 96: A of the cosmic ray effect on micro-electronics code. IEEE Transactions on Nuclear Science, 44, pp. 2150–2160, 1997.

[43] Badhwar, J.D., O'Neill, P. M., An Improved Model of GCR for Space Exploration Mission. Nuclear Tracks Radiation Measurements, 20, pp. 403 - 410, 1992.

[44] Townsend, L.W., Overview of Solar Energetic Particle Event Hazards to Human Crews. University of Tennessee, 2005.

[45] Mukhopadhyay, V., Structural configuration analysis of crew exploration vehicle concepts. 47th AIAA/ ASME/ASCE/AHS/ASC Structures, Structural Dynamics and Materials Conference, Newport, RI, 2006.

[46] Bannova, O., Bell, L., Radiation shielding design strategies for lunar minimal functionality habitability element. Acta Astronautica 67, (9-10):1103–1109, 2010.

[47] Rastegar, N., Eckart, P., Mertz, M., Radiation-induced cataract in astronauts and cosmonauts. Graefe Arch. Clin. Exp. Ophthalmol, 240, pp. 543–547, 2002.

[48] Hada, M., Sutherland, B.M., Spectrum of complex DNA damages depends on the incident radiation. Radiation Research, 165, pp. 223–230, 2006.

[49] Hellweg, C.E., Baumstark-Khan, C., Getting ready for the manned mission to Mars: the astronauts ' risk from space radiation. Naturwissenschaften, 94, pp. 517–526, 2007.

[50] Wilson, J.W., Miller, J., Konradi, A., Cucinotta, F.A., (Eds.), Shielding strategies for human space exploration. NASA CP 3360, 1997.

[51] Wilson, J.W., Tripathi, R.K., Qualls, G.D., Cucinotta, F.A., Prael, R.E., Norbury, J.W., Heinbockel, J.H, Tweed, J., De Angelis, G., Advances in space radiation shielding codes. Radiation Research, 43, S87–S91, 2002.

[52] Badhwar, G.D., Cucinotta, F.A., Depth dependence of absorbed dose, dose equivalent and linear energy transfer spectra of galactic and trapped particles in polyethylene and comparison with calculations of models. Radiation Research, 149, pp. 209–218, 1998.

[53] Shavers, M.R., Zapp, N., Barber, R.E., Wilson, J.W., Qualls, G., Toupes, L., Ramsey, S., Vinci, V., Smith, G., Cucinotta, F.A., Implementation of ALARA radiation protection on the ISS through polyethylene shielding augmentation of the Service Module Crew Quarters. Advances in Space Research, 34, pp. 1333–1337, 2004.

[54] Stormer, C., The Polar Aurora. Oxford University Press, 1955.

[55] Massachusetts Institute of Technology (2005). Final Report for NIAC Phase I Contract CP 04-0. Retrieved from http://www.niac.usra.edu/files/studies/final_report/988Hoffman.pdf

[56] John, S., Plasma Magnet for Deep Space Exploration and Radiation Shielding. Retrieved from http://www.niac.usra.edu/files/library/meetings/annual/oct05/917Slough.pdf.

[57] Tripathi, R.K., Wilson, J.W., Youngquist, R.C., Electrostatic Space Radiation Shielding. Advances in Space Research, 42, pp. 1043-1049, 2008.

[58] Science new (2005). A Forces Field for Astronauts ? Retrieved from http://science.nasa.gov/science-news/science-at-nasa/2005/24jun_electrostatics/

[59] Morse, P.M., Feshbach, H., Methods of Theoretical Physics. McGraw-Hill Company, New York, 1953.

[60] Townsend, L.W., Galactic heavy-ion shielding using electrostatic fields. NASA Technical Memorandum 86255, 1984.

[61] Vatankhah, A.R., Approximate solutions to complete elliptic integrals for practical use in water engineering. Journal of Hydrologic Engineering, 16, pp. 942-945, 2011.

[62] Rossi, B., Cosmic Rays. McGraw-Hill, New York, 1964.

[63] Wilson, J.W., Cucinotta, F.A, Shinn, J.L., Simonsen, L.C., Dubey, R.R., Jordan, W.R., Jones, T. D., Chang, C.K., Kim, M.Y., Shielding from solar particle event exposures in deep space. Radiation Measurements, 30, pp. 361-382, 1999.

[64] Reames, D.V., Particle acceleration at the sun and in the heliosphere. Space Science Reviews, 90, pp. 413–491, 1999.

[65] Webber, W.R., An evaluation of the radiation hazard due to solar particle events. Boeing Report D2-90469, Aerospace Division, The Boeing Company, 1963.

[66] ICNIRP, Guidelines on Limits of Exposure to Static Magnetic Fields. Health Physics, 96, pp. 504-514, 2009.

CURRICULUM VITAE

Trac K. Nguyen

Education:

Associate Degree in Science, 2004
Tidewater Community College, Virginia Beach, Virginia

B.S (Electrical Engineering), 2008
Old Dominion University, Norfolk, Virginia

M.S (Electrical Engineering), 2012
Old Dominion University, Norfolk, Virginia

Experience:

NASA Langley Research Center, Graduate Student Research Program, January 2008 – July 2008.

Publications:

Christopher S. Garcia, Abedin M. Nurul, Syed Ismail, Shiv K. Sharma, Anupam K. Misra, Trac Nguyen, Hani Elsayed–Ali, "Study of minerals, organic, and biogenic materials through time-resolved Raman spectroscopy," Proc. SPIE 7312 , Advanced Environmental, Chemical, and Biological Sensing Technologies VI, 731210. (April, 30 2009)